The physical hydrology of ore-forming magmatic-hydrothermal systems

This is the Green Open Access version of: Weiss, P., 2014. The physical hydrology of ore-forming magmatic-hydrothermal systems. *Society of Economic Geologists, Inc.,* Special Publication 18, pp. 59–75
Original publication see: https://doi.org/10.5382/SP.18.04

The physical hydrology of ore-forming magmatic-hydrothermal systems

Philipp Weis

Institute of Geochemistry and Petrology, ETH Zurich

Clausiusstrasse 25 (NW F 84), 8092 Zürich, Switzerland

Phone +41 44 632 0483, Fax +41 44 632 1827, e-mail: philipp.weis@erdw.ethz.ch

Abstract

Classifications of magmatic-hydrothermal ore deposits are largely geochemical, based on metal associations and characteristic alteration types, but the process of metal enrichment is primarily controlled by the physical hydrology of fluids flowing through rocks. Physical hydrology plays a decisive role in forming distinct ore deposit types, including volcanogenic massive sulfide deposits at mid-ocean ridges or submarine arc volcanos, porphyry-style ore deposits in continental collisional arcs, and epithermal vein and replacement deposits. Results from simulations of magmatic-hydrothermal systems using a new numerical modeling platform for thermohaline convection are used to determine the implications for ore formation in light of the different structural styles, timing and igneous characteristics of major magma-related ore deposit types. Thermal convection, volatile expulsion, and salt-water dynamics are shown to be the first-order hydrological components, and different combinations or successions of general hydrological patterns characterize particular ore-forming systems.

Due to the nonlinear properties of fluids and rocks as a function of pressure, temperature and composition, the physical behavior of hydrothermal systems can be counterintuitive, and understanding their self-organization requires numerically rigorous models. Thus, mid-ocean ridge hydrothermal systems do not involve broad-scale lateral infiltration of seawater; instead, focused warm downflow in the immediate vicinity of hot upflow zones provides a more efficient mechanism for metal leaching and ore-formation in Cyprus-type massive sulfide deposits. Phase separation in submarine magmatic-hydrothermal systems can lead to a decoupling of vapor-dominated venting, which is expected to favor sulfur-complexing of some metals leading to the formation of Au-rich chimneys, whereas chloride-complexing metals may precipitate during the waning stages, favoring the formation of base-metal rich sulfide deposits from negatively buoyant brines. Porphyry copper mineralization is localized by a self-stabilizing hydrological front, located at the transition from brittle to ductile rock behavior and controlled by the heat balance between an external convective cooling engine and an overpressured magmatic fluid plume. This

hydrological divide also provides a mechanism for the transition to epithermal-style deposits where magmatic and meteoric fluids mix on ascent to the surface.

1. Introduction

Magmatic-hydrothermal systems in the upper crust are the physical drivers for many ore-forming processes, leading to chemical enrichment of elements to economic grades (Hedenquist and Lowenstern, 1994; Kesler, 1994). Hydrothermal ore formation requires that the respective elements can be extracted from a large source volume and transported in aqueous solutions (Heinrich and Candela, 2014). This fluid flow ideally becomes focussed and provides a steady precipitation mechanism within the flow path. Hydrothermal convection is strongest in the vicinity of magmatic activity, which acts as a heat source for ambient fluids in the adjacent host rock and adds variable amounts of magmatic volatiles (Burnham and Ohmoto, 1980; Candela, 1991; Hedenquist and Lowenstern, 1994; Henley and McNabb, 1978; Richards, 2013; Wilkinson, 2013).

Classification of hydrothermal ore deposits associated with upper-crustal magmatism has traditionally been based on metal associations and characteristic alteration (e.g. Kesler, 1994; McCuaig and Kerrich, 1998). However, these chemical characteristics are ultimately determined by the physics of fluid flow through rocks, which is fundamentally different in volcanogenic massive sulfide, porphyry copper and epithermal gold deposits (e.g. Hannington et al., 2011; Hannington, 2014; Henley and Ellis, 1983; Sillitoe, 2010). These differences are dominated by 1) the size, depth and composition of the magmatic source, 2) the pressure-, temperature- and composition-dependence of fluid properties, 3) permeability distribution and evolution, 4) rock mechanics and crustal stress state, and 5) chemical fluid-rock interactions.

This paper emphasizes physical hydrology as a critical control for chemical enrichment in ore-forming magmatic-hydrothermal systems, based on recent numerical modelling and comparison with active hydrothermal systems involving, in varying proportions, meteoric water, magmatic fluids and seawater.

2. Fluid Flow

Conservation of mass, energy, and momentum are the principal physical laws that characterize fluid flow in magmatic-hydrothermal systems (e.g. Ingebritsen et al., 2010; Ingebritsen et al., 2006). An undisturbed stagnant state of subsurface fluids is referred to as hydrostatic, where fluid pressure equals the load of an overlying interconnected water column. The driving forces for hydrothermal systems are perturbations of this balance, for instance by injection or withdrawal of fluids, or changes in fluid density due to temperature or compositional changes (e.g. Cathles, 1977; Gunnarsson et al., 2011; Hanson, 1995; Hayba and Ingebritsen, 1997; Henley and McNabb, 1978; Norton and Knight, 1977). Fluid flow is also driven by horizontal pressure gradients, which can result from topographical differences (Sammel et al., 1988) or horizontal density gradients between a hot upflow and a cold recharge zone (e.g. Cathles, 1977; Hayba and Ingebritsen, 1997; Norton and Knight, 1977). Fluid fluxes are further constrained by the resistance to flow, which is determined by the permeability of the rock and the viscosity of the fluid (Ingebritsen et al., 2006). The governing equations for fluid flow according to Darcy's law in porous and fractured media are formulated and explained in the Appendix.

2.1. *Multi-component, multi-phase flow*

The physical hydrology of magmatic-hydrothermal systems is strongly influenced by phase separation of variably miscible, compressible fluids (Ingebritsen et al., 2010). The boiling curve of pure H_20 extends from 100°C at atmospheric pressure to the critical point of water at a temperature of 374°C and a fluid pressure of 22.1 MPa (Haar et al., 1984). Fluids intersecting this curve on their flow path separate into a low-density vapor and a high-density liquid which can subsequently physically separate owing to different phase velocities and directions. Adding salts like NaCl and other solutes or gaseous components like CO_2 extends the areas of multi-phase conditions to considerably higher temperatures and fluid pressures (Driesner, 2007; Driesner and Heinrich, 2007; Ingebritsen et al., 2010). Both NaCl and CO_2 are abundant in ore-forming magmatic-hydrothermal systems.

2.2. *Numerical modeling*

Given the complexity of the coupled physical and chemical processes and the non-linear properties of materials (rocks, fluids), the conservation equations are usually impossible to assess with analytical models. Conceptual models can identify single aspects of the hydrological dynamics that may evolve from these coupled equations. Numerical process modeling then provides a comprehensive and physically rigorous method to quantify multi-phase fluid flow in the subsurface (Ingebritsen and Appold, 2012; Ingebritsen et al., 2010). There are several codes that solve the equations with different numerical approaches (e.g. Bani-Hassan et al., 2012; Coumou et al., 2009b; Geiger et al., 2004; Keating et al., 2002; Kipp et al., 2008; Kissling, 2005; Lewis and Lowell, 2009; Pruess, 2004; Weis et al., 2014). Most of them are still of limited applicability to magmatic-hydrothermal systems as the strongly non-linear behavior of fluid properties is challenging for any numerical method (Weis et al., 2014). Simulations also require that accurate and comprehensive thermodynamic models are available for the respective fluid systems over the wide ranges in temperature or enthalpy, pressure and composition, which is so far only the case for the H_20-NaCl system (Ingebritsen et al., 2010).

The examples of simulations presented in this paper were calculated with an implementation of the Complex Systems Modeling Platform (CSMP++; Matthai et al., 2007) for thermohaline convection, which includes an accurate thermodynamic representation of properties of salt water for magmatic-hydrothermal conditions (up to 1,000 °C, 500 MPa and 100 wt% NaCl; Driesner, 2007; Driesner and Heinrich, 2007). A detailed description of the method including benchmarks and code comparison with other well-established codes can be found in Weis et al. (2014). Although the nonlinear nature and complexity of hydrothermal systems can lead to counterintuitive results, numerical simulations with relatively simple model configurations often show a tendency towards self-organization. Many aspects of temporal and spatial variability observed in natural systems can be explained by basic hydrological patterns that depend more on the general geological setting than the specific sites.

3. General Patterns

The physical hydrology of magmatic-hydrothermal systems can be distinctly different depending on whether magmatic activity acts as a conductive heat source for convection, or whether hot volatiles are expelled from a magma chamber into the host rock (Fig. 1). The composition of the fluids also plays a major role, particularly due to the different salinities of meteoric water, magmatic fluids and seawater, which affect behavior during phase separation (Fig. 2 - 4). We can

distinguish three main drivers of magmatic-hydrothermal systems with increasing level of complexity: thermal convection, volatile expulsion, and salt water dynamics.

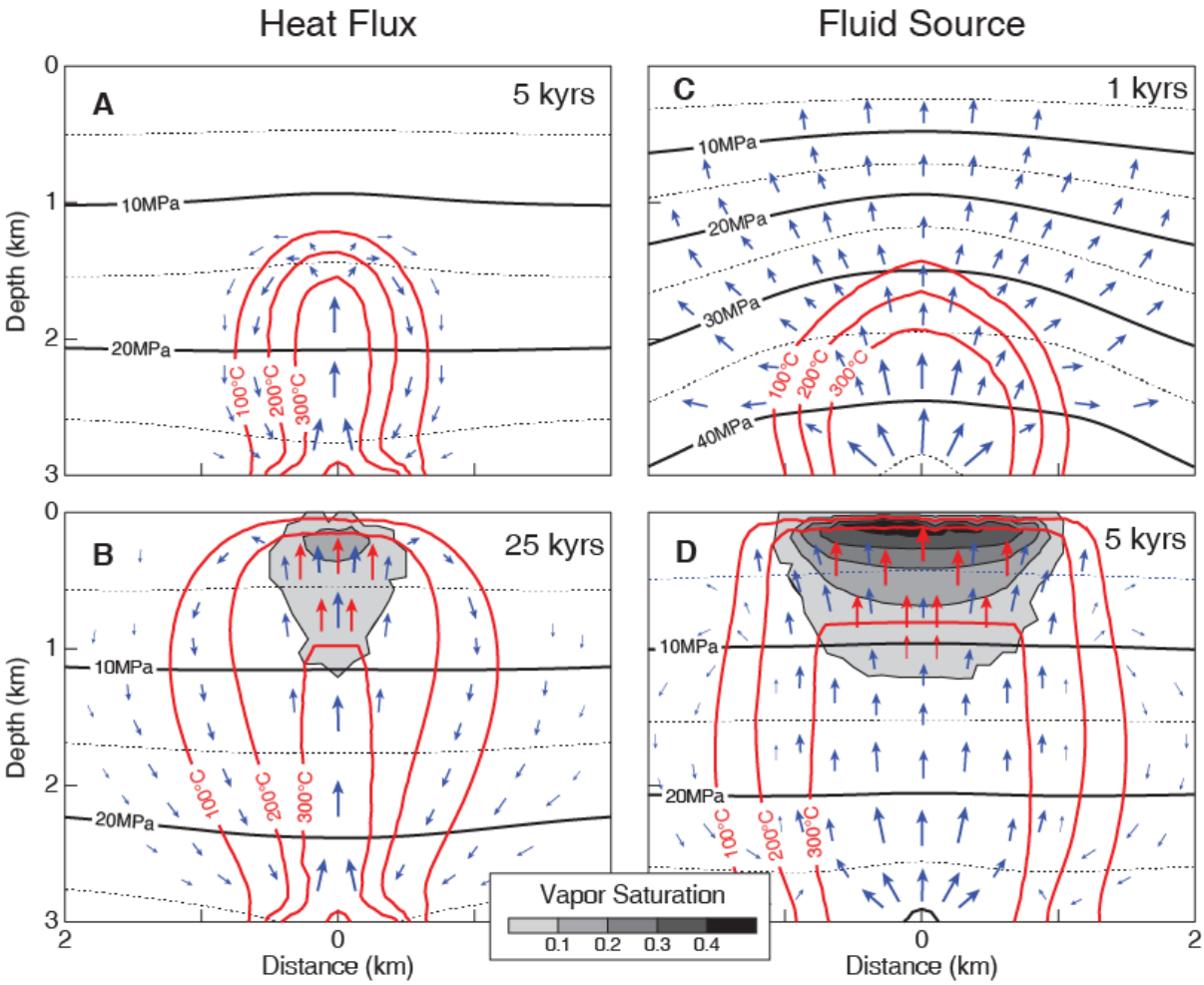

Fig. 1. Propagation of a thermal front during slow buildup of thermal convection (left) compared with the rapid advance resulting from forceful expulsion of magmatic fluid (right). The contrasting evolution of the two types of hydrothermal systems is calculated for the same geometry, a two-dimensional 9 x 3 km vertical section of the upper crust of which the figures only show the inner part of 4 km width. The top boundary represents the Earth's surface at 10°C and atmospheric pressure. Permeability is homogeneous and isotropic with a constant value of $k=10^{-15}$ m^2, typical for tectonically active upper crust (Manning and Ingebritsen, 1999). The pore space of the domain is initially saturated with pure water of 10°C and hydrostatically pressured. The magma chamber below the bottom boundary imposes an elevated heat flux (left) or a magmatic fluid source (right). The purely conductive heat source (left; **A**, **B**) uses an extra heat flux of 9 W m^{-2} through the central 1 km segment of the bottom boundary, providing a total heat input of 9 kW for the two-dimensional model with a nominal thickness of 1 m. Results are shown after 5000 years (**A**) and 25000 years (**B**) of simulation time. Magmatic fluid expulsion (right; **C**, **D**) imposes a flux of pure water through the center of the bottom boundary with a rate of 0.04 kg s^{-1} and an enthalpy of 1.5 MJ kg^{-1} (total heat input of 60 kW); snapshots are shown after 1000 years (**C**) and 5000 years (**D**). Temperatures are plotted as red lines and fluid pressure as black lines. Grey-shaded areas indicate zones where phase separation to liquid and vapor occurs, scaled by the extent of vapor saturation (volume fraction vapor / vapor + liquid in the pore space). Fluid flow is illustrated by schematic arrows for the liquid (blue) and vapor phases (red), with thickness and size of arrows indicating differences in velocities. Modified from Weis et al. (2014).

3.1. Thermal convection

Localized heat input causes differences in fluid density and buoyancy-driven fluid flow. In the initial stages of a convecting system, a thermal plume starts to rise due to heating and expanding fluids near the heat source (Fig. 1A). These lower density fluids make their way toward the surface, leading to fluid pressures that are slightly higher above the thermal front and an outward-oriented horizontal pressure gradient. In the heated part of the upflow zone, fluid pressures are

slightly lower than in the recharge areas, due to the lower density of the fluids, resulting in a horizontal pressure gradient that is orientated inward. During this initial phase of the thermal plume, a convection cell develops within the crust. Heat and mass transport are decoupled as the energy of rising heated fluids is consumed to heat the host rock above the thermal front. With fluid density increasing upon cooling, these fluids eventually sink back to greater depths and are reheated. As a consequence, the same mass of water can be involved multiple times in collecting heat from the magma chamber and heating the overlying rock.

This pattern changes with breakthrough of the thermal plume to the surface. In the example (Fig. 1B), ascending hot fluids intersect the boiling curve at about 1 km depth. From this point upwards, the temperatures of the upflow zone follow the boiling curve. The ascending single-phase fluid separates into a high-enthalpy, low-density vapor and a lower-enthalpy, higher-density liquid, with volumetric saturations of the vapor phase increasing towards the surface. The final stage is a quasi-steady state, with a convection cell that includes fluids entering and leaving through the surface and only a minor liquid component convecting within the crust.

3.2. Volatile expulsion

During the initial stages of a forceful magmatic-fluid injection, propagation of the thermal front is accompanied by a strong pressure anomaly that extends radially outward from the injection point, pushing away ambient fluids to accommodate the injected hot fluids (Fig. 1C). The pressure increase affects areas that are kilometers away from the thermal plume, because diffusion of fluid pressure is significantly faster than heat and mass transport (far-field pressurization).

With advancement of the thermal plume and its breakthrough to the surface, this pressure anomaly slowly decreases (Fig. 1D). In the quasi-steady state of the example, the pressure distribution is close to cold hydrostatic. However, depending on the source rate and permeability, the system may maintain a pressure anomaly or develop a more convective pattern. In the example, only a very minor component of the liquid phase sinks back to greater depths, while almost all of the injected fluid vents as liquid or vapor through the surface. Again, the ascending hot single-phase fluid starts to boil at a depth of about 1 km and temperatures follow a boiling-curve-with-depth profile while vapor saturations increase towards the surface.

3.3. Salt water dynamics

Phase separation of saline fluids can result in a complex and dynamic hydrology that may never reach a steady state. Owing to the fact that the addition of NaCl widens the two-phase field to higher temperatures and pressures, magmatic fluids with a moderate salinity of initially 1 wt% NaCl injected at 3 km depth immediately phase-separate into a two-phase mixture of a low-salinity, low-density vapor and a high-salinity, high-density liquid (Fig. 2). The vapor phase physically separates from the brine, leading to a rapid increase in bulk salinity to values above 30 wt% NaCl near the injection location after only 500 years of simulation time (Fig 2A). This high-salinity two-phase region is surrounded by a zone of pure vapor (Fig. 2B).

Similar to the pure-water case, propagation of the thermal front with saline fluids is accompanied by a significant pressure anomaly during the early stages (Fig. 2A), which relaxes with breakthrough of the plume to the surface (Fig. 2C). Together with continuing phase separation at the injection point, this decrease in fluid pressure leads to saturation in solid halite and a significant change in phase distributions (Fig. 2D). The field of vapor-liquid coexistence at the injection point is now surrounded by a ring of three-phase vapor-liquid-halite coexistence. Above

that ring, a vapor-dominated plume with minor portions of solid halite extends to the surface, flanked by corridors of two-phase vapor-liquid upflow.

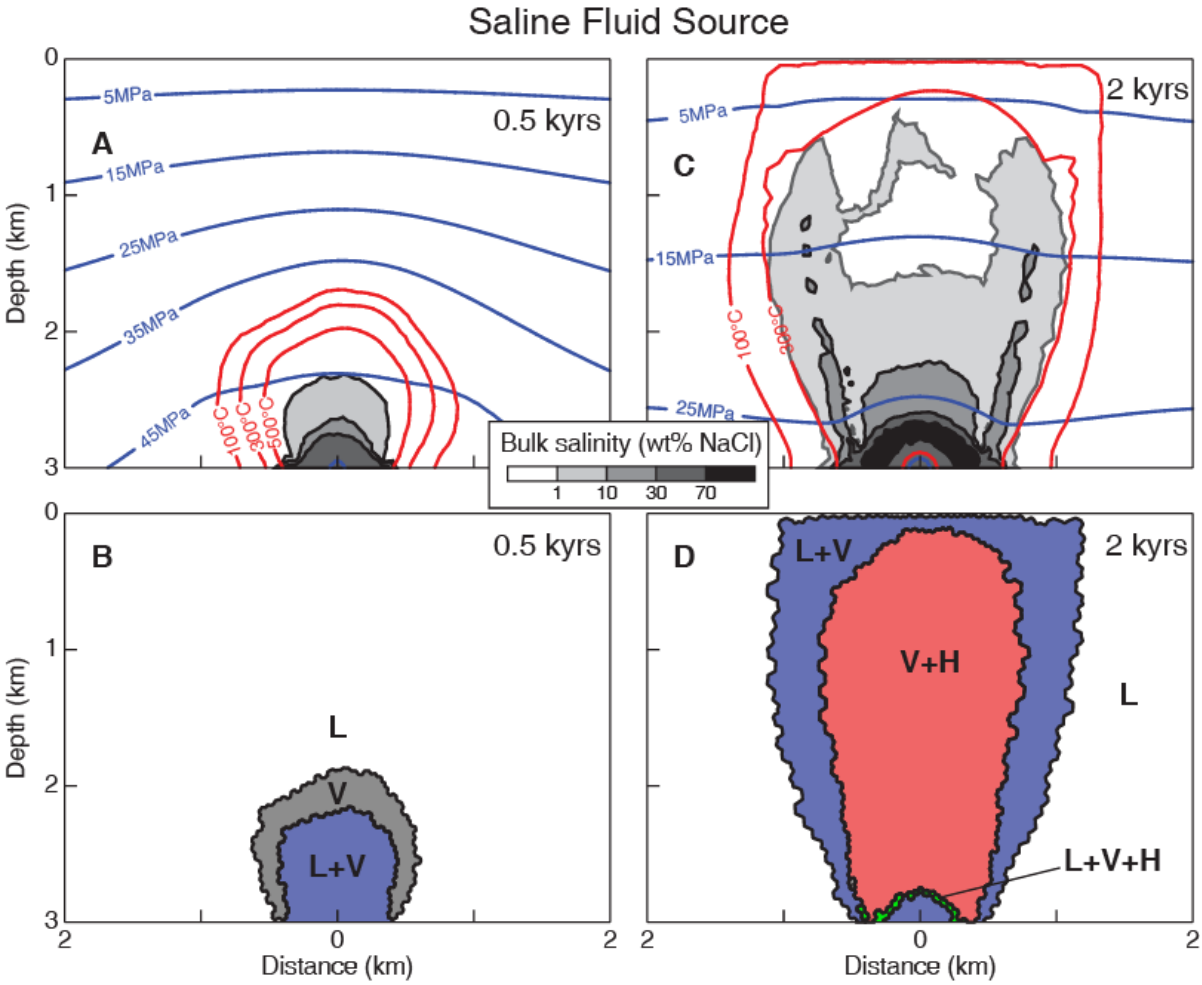

Fig. 2. The impact of salt on the temporal and spatial evolution of a magmatic-hydrothermal system, resulting from forceful expulsion of a low-salinity (1 wt% NaCl) magmatic fluid into a previously pure water saturated rock. Successively different salinity distributions (top) and fluid phase states including liquid, vapor and halite saturation (bottom) result after 500 years (**A** and **B**) and 2000 years (**C** and **D**) of simulation time. Magmatic degassing is parameterized by injection of a fluid with the same source rate as in Fig. 1C and D (0.04 kg s^{-1}), but with an enthalpy of 3 MJ kg^{-1} and a salinity of 1 wt% NaCl. Bulk salinity of the fluid is indicated by the grey-shaded areas, temperatures are plotted as red lines and fluid pressure as blue lines (**A** and **C**). Fluid phase states (**B** and **D**) are illustrated by coexistence fields of vapor (V), liquid (L) and/or halite (H). Modified from Weis et al. (2014).

Solid halite in these simulations is considered to be immobile and to reduce the pore space and permeability available for the mobile vapor and liquid phases (Appendix; Weis et al., 2014). Continuing precipitation of halite therefore leads to pulsating fluid flow. Due to the associated permeability reduction, fluids added at the bottom are prevented from escaping, resulting in a pressure buildup. This pressure increase may eventually move the fluids from halite-saturated phase states into the vapor-liquid coexistence field (Driesner and Heinrich, 2007). Re-dissolution of salt then increases the relative permeability, allowing a new batch of fluid to ascend to shallower depths. The subsequent release of pressure results in further halite precipitation and repeated reduction in permeability.

This pulsating behavior causes episodic upward propagation of the salt front (Fig. 3A). Although the salinity of the input fluid is only 1 wt% NaCl, bulk salinities between 2 and 3 km depth reach values approaching 100 wt% NaCl throughout the 10,000 years of simulated fluid expulsion.

Salinities increase only slowly in the upflow zone of vapor-halite coexistence, and upflow in the vapor-liquid coexistence field with slightly elevated bulk salinities is limited to a narrow band on the flanks of the vapor-halite field. Most of the salt added to the system is retained in the crust and only slowly vented through the surface (Fig. 3B). The pulsating behavior of the hydrothermal system is also reflected by the temporal changes in bulk salinity of the fluid in which the salt mass is contained (Fig. 3B).

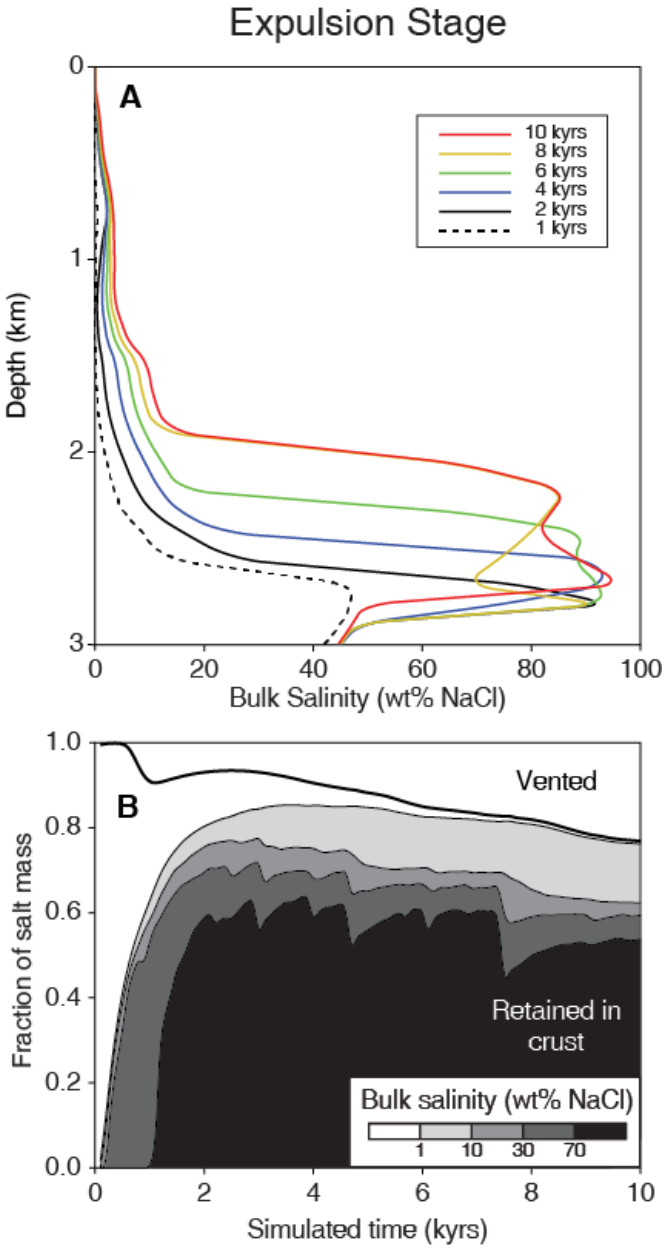

Fig. 3. Injection of weakly salt-bearing magmatic fluid into previously salt-free rocks of fixed permeability leads to vapor separation and accumulation of increasingly saline liquid (brine) just above the fluid source; only a small fraction of injected salt reaches the surface due to the negative buoyancy of the increasingly salty brine. **A** shows the upward propagation of a salinity front, as salt gradually accumulates in the crust above the injection point at 3 km depth. The graph shows the bulk salinity of the fluid along the vertical center line of the model domain of Figure 2, for different snapshots in time. **B** shows the fraction of total injected salt mass that either vents through the surface or is retained in the crust; e.g., after 2000 years of simulation time, less than 10% of the salt mass injected has been vented, while the remaining >90% are retained as heavy brine in the crust. The grey shading differentiates the bulk salinities of the fluid in which the salt mass is contained. Modified from Weis et al. (2014).

Switching off the magmatic fluid source after 10,000 years of simulation time results in gradual cooling of the hydrothermal system. During the early waning stage, the remaining heat drives

thermal convection of ambient fluids that dilute the accumulated salt. The magmatic salt mass can be transported to the surface as warm brines with salinities of up to 20 wt% NaCl (Fig. 4A). With further cooling, the remaining brines get too heavy to ascend and about half of the magmatic salt added during the injection phase is retained in the crust even after a simulation time of 100,000 years (Fig. 4B). During the later waning stage, salt that accumulated around the former injection point still gets progressively diluted with time (as documented by the graphs for bulk salinity at 50 and 100 kyrs in Fig. 4A and the overall decrease in bulk salinities with time in Fig. 4B), but the brines rather spread laterally and remain at the base of the modeling domain (as documented by the almost constant ratio between vented and retained salt mass in Fig. 4B).

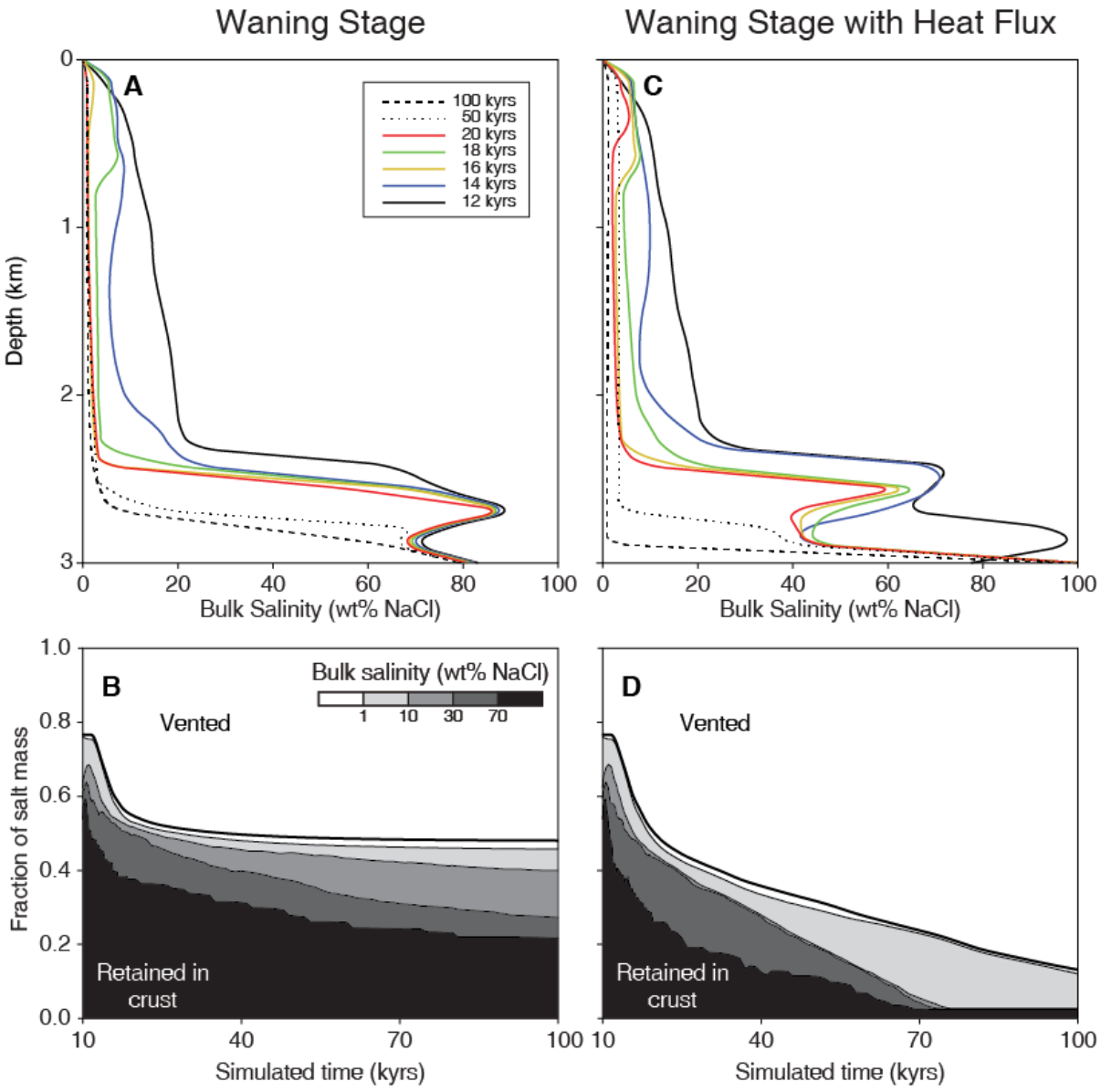

Fig. 4. Salt accumulated as a result of forceful magmatic fluid injection can only be mobilized by sustained thermal convection after magmatic injection has stopped, which is likely during sub-solidus cooling of magmatic intrusions. This process of 'brine mining' has been simulated by extending the calculations shown in Figure 2, beyond the initial 10 kyrs of weakly saline fluid injection that built up a large brine reservoir at depth (Fig. 3). Without localized heat input (simulation results in **A**, **B**), accumulated salt is retained in the crust indefinitely as heavy brine. However, with a moderately elevated heat flux of 1 W m^{-2} localized at the center 1 km of the bottom boundary (simulation **C**, **D**), thermal convection can mobilize most of the accumulated salt and flush it towards the surface as salty hydrothermal liquid with salinities of up to 20 wt% NaCl. As in Figure 3, graphs at the top (**A**, **C**) show bulk salinity of the fluid along the vertical center line; **B** and **D** show the fraction of total salt mass injected that has either vented through the surface or is retained in the crust with grey shading to show bulk salinities of the fluid in which the salt mass is contained.

In an alternative waning stage scenario, the magmatic fluid source is also switched off after 10,000 years of fluid injection, but a moderately elevated heat flux is applied to the center of the bottom boundary, simulating a remnant temperature anomaly from a cooling pluton at depth (Fig. 4C and D). The additional heat is able to maintain a convection cell that keeps the heavy brines mobile and results in slow but steady venting of the majority of the magmatic salt during the 100,000 years of simulation time (Fig. 4D).

3.4. Active and fossil ore-forming systems

The general patterns of thermal convection, volatile expulsion, and salt water dynamics presented above are the main ingredients explaining fluid flow at active hydrothermal sites or in reconstructing the hydrology of fossil ore-forming systems. Generic numerical simulations (as shown with examples in the following sections) aim to identify first-order hydrological controls and quantify mass and heat fluxes by keeping the model as simple as possible. Field observations and conceptual models are used to configure the simulations. Available measurements can then be used to further constrain the numerical model, and to evaluate whether the hydrology predicted by the model can reproduce key observations or needs to be refined. The following examples show results of simulations with our CSMP++-based model for thermohaline convection. Details of the model configurations and simulations can be found in the cited references (Coumou et al., 2009a; Coumou et al., 2008; Coumou et al., 2009b; Gruen, 2011; Gruen et al., 2012; Weis et al., 2012).

4. Volcanogenic Massive Sulfide Deposits

At divergent plate margins, such as mid-ocean ridge systems, predominantly basaltic magmatism is the heat source driving convection (Halbach et al., 2003). Fluids are heated near an axial magma chamber, which reduces fluid density and results in upflow of hydrothermal fluids that vent back to the ocean at black smoker fields. These magma chambers are elongated in the orientation of the ridge axis and are believed to be episodically refilled (Baker and Urabe, 1996; Ginster et al., 1994; Ramondenc et al., 2006).

4.1. Black smoker vent fields

Three-dimensional numerical simulations show that hydrothermal systems at mid-ocean ridges can self-organize into pipe-like upflow zones (Coumou et al., 2009a; Coumou et al., 2008) and that the spacing of predicted black smoker vent fields, as well as their venting temperatures, reproduce observations from natural systems (Glickson et al., 2007; Johnson et al., 1993; Lowell et al., 1995; Van Ark et al., 2007) (Fig. 5). The hydrologic configuration results from the nonlinear properties of water. The upflow zone is dominated by ascending fluids at about 400°C, where water develops the strongest buoyancy-driven convection (Jupp and Schultz, 2000). The hot fluids of the upflow zone also conductively heat the surrounding rock and fluids. Increasing water temperature from 10°C to 200°C results in decreases in the fluid density by only about 10%, whereas viscosity decreases by almost an order of magnitude, which has the same effect as increasing permeability by an order of magnitude (see Appendix).

As a consequence, two thirds of the recharge is focused into a zone in the immediate vicinity of the upflow, optimizing heat and mass flux in a cylindrical configuration (Coumou et al., 2009a; Coumou et al., 2008). In Figure 5B, the focused downflow is indicated by the higher pore velocitities in the region between the 100°C to 300°C isotherms (gray arrows) compared to the colder recharge areas (blue arrows) at further distance from the upflow zone (red arrows). This

self-organization maintains a state of least hydraulic resistance to maximize heat-transport efficiency; counterintuitively, during this process, recharging fluids become pre-heated by the ascending fluids before they enter the basal area in contact with the magmatic body.

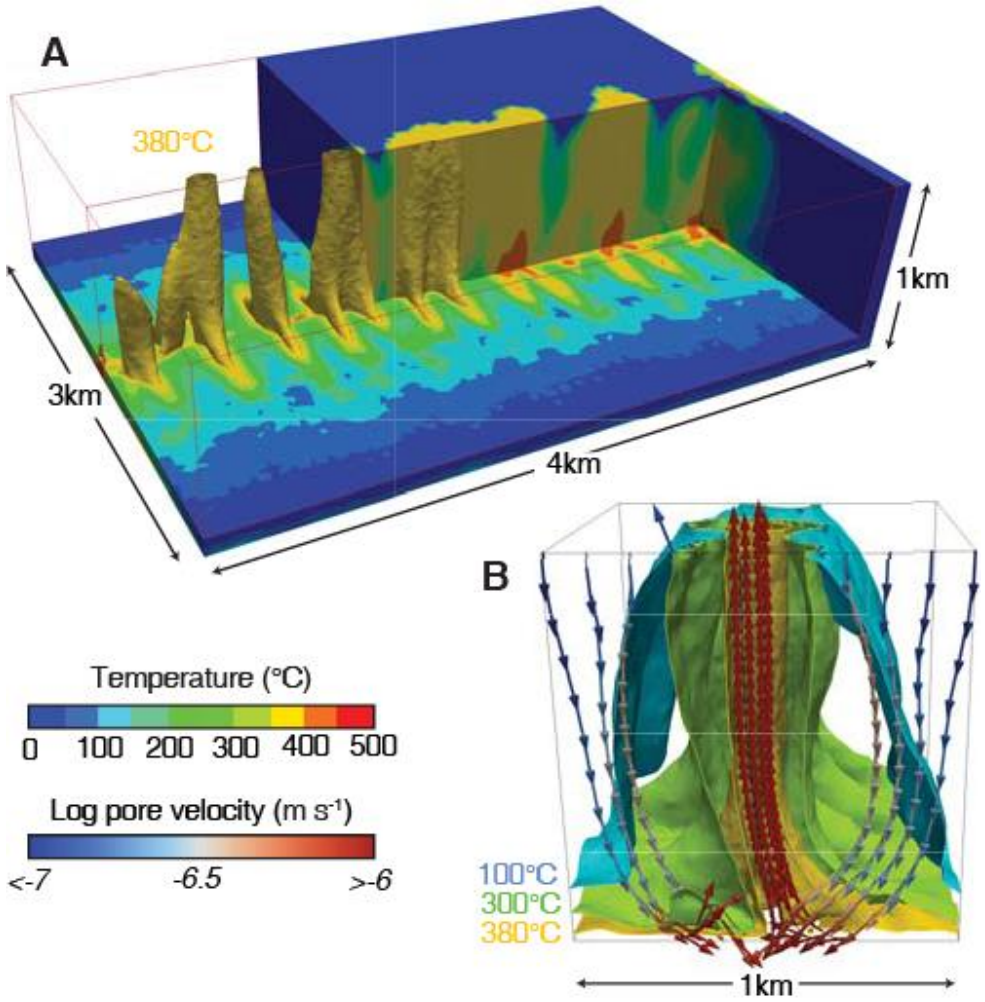

Fig. 5. Three-dimensional simulation of the hydrology of black smoker vent fields at mid-ocean ridges (after Coumou et al., 2008). Self-organisation of upflow zones in linear tubes, despite continuous heat input along the spreading axis, is a result of non-linear physical properties (density and viscosity) of heated liquid water. Thermal convection with pure H_20 as a proxy for seawater is simulated with homogeneous, isotropic rock properties for a section of the oceanic crust, a water depth of 2500m typical for fast- to intermediate spreading ridges and a Gauss-shaped heat flux profile approximating the geometry of the magma chamber. **A)** Temperature distribution after 140 years of simulation time. **B)** An excerpt showing pore velocity arrows along selected streamlines, illustrating the focused down-flow of warm fluids surrounding the hot, pipe-like up-flow zone.

4.2. Salinity variations

Salinities of venting fluids at black smokers can vary significantly in time and space. At fast- to intermediate-spreading ridges, temporal variations in venting salinity result from episodic brine flushing, or simultaneous venting of vapor and brine in the same black smoker field or even from the same black smoker only (Butterfield et al., 1990; Massoth et al., 1989; Oosting and Von Damm, 1996; Von Damm et al., 1997; Von Damm et al., 2003; Von Damm et al., 1995). Two-dimensional numerical simulations of across-axis convection of salt water show that a two-phase upflow zone can span the depth range from the axial magma chamber to the vents (Coumou et al., 2009b) (Fig. 6A). Depending on permeability, vapor can be volumetrically dominant within this zone, resulting in vent salinities below seawater salinity. At most times, liquid is only present as a wetting phase in the pore space, which means that the high-salinity brine becomes immobile. However,

continuous condensation within the upflow zone results in accumulation of increasingly more brine until the liquid saturation exceeds a threshold value (see discussion of residual permeability in the Appendix), whereupon a higher-salinity brine phase can ascend and temporarily increase venting salinity.

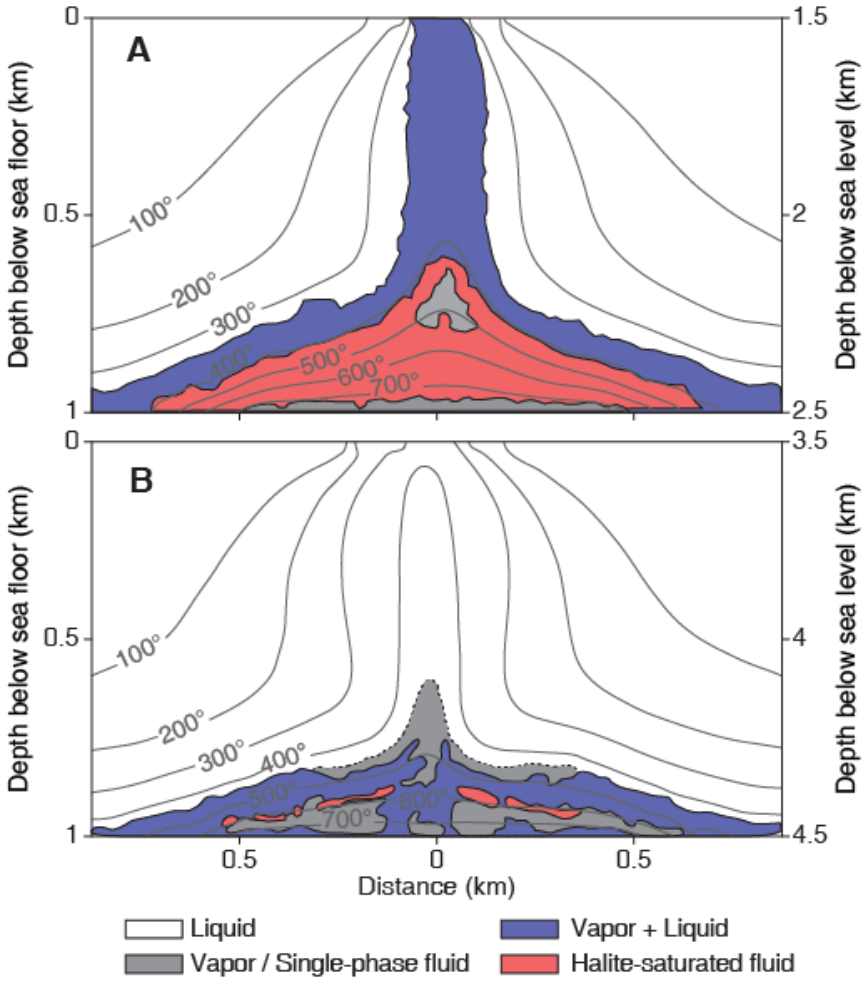

Fig. 6. Fluid phase relations at mid-ocean ridge systems resulting from seawater salinity without input of any magmatic fluid (modified from Coumou et al., 2009b; Weis et al., 2010). The figures show the distribution of phase states and temperatures at a quasi-steady state. Two-phase fluids (more saline liquid and less saline vapor) reach the seafloor at fast-spreading ridges due to their typically shallow water depths (1.5 km assumed for simulation **A**). By contrast, hydrothermal systems at slow-spreading ridges operate at greater water depths of around 3.5 km, so that the greater water pressure limits phase separation to the base of the hydrothermal system and boiling fluids do not vent to the seafloor (**B**).

At slow-spreading ridges, this episodic brine flushing associated with two-phase processes is suppressed by the higher fluid pressures imposed by the greater ocean depth. Here, boiling occurs only at the base of the system (Fig. 6B). Phase separation near the axial magma chamber leads to ascent of vapor-dominated fluids, which contract to a low-salinity liquid-like fluid at the vent site (without undergoing a phase change), and accumulation of a brine layer at depth. Only after shut down or waning of the heat source can this brine layer be slowly mined, causing an extended period of venting of fluids with moderately elevated temperatures and salinities well above sea water. Both types of venting (below and above sea water salinities) have been observed at slow-spreading ridges, and may reflect whether the underlying system is still active or in a waning stage (Butterfield et al., 1994; Charlou et al., 1996; Chiba et al., 2001; Edmonds et al., 1996; Gallant and Von Damm, 2006; James et al., 1995; Seyfried et al., 2003; Von Damm et al., 1998).

With the addition of magmatic fluids released from more felsic magmas, such as at submarine arc volcanos (cf. de Ronde et al., 2005; Gruen et al., 2012), the hydrothermal system may follow the same principles as the generic simulation for salt-water dynamics (Fig. 2 to 4) with vapor-dominated venting during the main stage of fluid release and brine mining during the waning stage (Gruen, 2011). Because metals preferentially partition into the exsolving fluid phase rather than the melt or the rock, magma chamber dynamics inherently tap a large source volume and focus fluid flow (Heinrich and Candela, 2014). To ensure chemical enrichment, the ascent of magmatic volatiles through the overlying rock has to remain focussed and the hydrologic system has to provide a mechanism for ore deposition.

4.3. Implications for ore formation

Conceptual models of mid-ocean ridge hydrothermal systems usually infer that the largest possible difference in fluid density (i.e. temperature) is the primary driving force for convection (e.g. Johnson et al., 1993). This concept implies that the so-called reaction zone, where fluids are hot enough for significant chemical fluid-rock reaction, is restricted to the immediate vicinity of the magma chamber at the base of the hydrothermal system (e.g. Alt, 1995). However, the warm downflow in the vicinity of the hot upflow zone shown by the 3D modeling (Fig. 5) is able to leach copper and other metals from the ocean crust much more efficiently than cold recharge zones at further distance (Coumou et al., 2008; Hemley et al., 1992; Seyfried and Ding, 1995). Metals can then be transported to vent sites at black smoker fields, where ore minerals precipitate upon cooling in contact with ocean waters (Hannington et al., 2011; Hannington, 2014). With fluid residence times as short as three years, mass-balance calculations of the 3D modeling results suggest that the system would be able to form an average massive sulfide deposit with 0.2 Mt Cu within 100 to 1,000 years (Coumou et al., 2008).

Phase separation and brine accumulation at depth can also have a significant influence on ore formation, because solubility of metals increases both with temperature and salinity, which results in a larger capacity of warm brines to leach metals from the crust and transport them to a precipitation site where the fluids are cooled and diluted (Foustoukos and Seyfried, 2007; Hannington, 2014; Hemley et al., 1992, Yardley, 2005).

During phase separation of the ascending fluids, sulfide-complexed metals such as Au may preferentially become enriched in the vapor phase (Heinrich et al., 1999; Pokrovski et al., 2008), which vents during the main stages of magmatic activity. Chloride-complexed base metals may be temporarily stored in the heavy brine, which is retained in the crust during the active magmatic phase and can be transported to the seafloor during the waning stage with salinities greater than 10 wt% NaCl (Coumou et al., 2009; Gruen, 2011), which agrees with salinities assumed for the formation of brine pools. The heavy brines may sink into depressions on the seafloor and precipitate their metal contents upon cooling and in combination with an additional sulfide source, forming layered massive sulfide deposits (e.g. Hannington, 2014; Solomon et al., 2004).

5. Porphyry and Epithermal Deposits

Continental collisional arcs host the world's largest resources of copper, gold and numerous other metals in porphyry and epithermal deposits of variable dimensions (Richards, 2013; Sillitoe, 2010). The broad similarity of these types of deposits requires a comparatively uniform and simple mechanism for ore formation (Richards, 2013; Sillitoe, 2010; Wilkinson, 2013). For generic simulations of the hydrology of porphyry copper systems (Weis et al., 2012), our model has been constrained with geological observations and conceptual models, in particular from the Yerington

Batholith in Nevada, and the Bingham Canyon Cu-Mo-Au porphyry deposit in Utah (Dilles, 1987; Dilles and Einaudi, 1992; Gruen et al., 2010; Landtwing et al., 2005; Redmond et al., 2004; Weis et al., 2012). The initially hot magma chamber (900°C), with a volume of about 100 km^3 at 5 km depth, is cooled by conduction and advection of ambient fluids. Magmatic fluid production is calculated as being proportional to the crystallization rate of the pluton during cooling below a solidus temperature of 700°C, and fluids are injected into the host rock through a cupola in the roof of the magma chamber (Burnham and Ohmoto, 1980; Candela, 1991; Dilles, 1987; Weis et al., 2012).

5.1. Dynamic permeability

Simulations with static system-scale permeabilities were not able to reproduce the characteristic fluid states documented by numerous fluid inclusion studies, nor did they describe an efficient precipitation mechanism. We therefore assembled a dynamic permeability model by mapping existing models for permeability, stress state, and failure conditions of the continental upper crust to our porous medium approach (Weis et al., 2012). This model has the following characteristics:

Permeability generally follows a depth-dependent profile characteristic of tectonically active continental crust (Manning and Ingebritsen, 1999).

This permeability profile is linked to a critically-stressed brittle crust (Zoback et al., 2002); that is, differential stress increases with depth, resulting in failure criteria for fractures at moderately elevated, near-hydrostatic fluid pressures (Cox, 2010).

At elevated temperatures, increasingly ductile rock behavior leads to the loss of interconnected pore space, resulting in lower permeability values (Fournier, 1999; Hayba and Ingebritsen, 1997). At the same time, differential stress relaxes, resulting in a near-lithostatic failure criterion (Cox, 2010) for temperatures above the brittle-ductile transition, which we assume to occur between 360°C and 500°C (Hayba and Ingebritsen, 1997).

Whenever fluid pressures exceed the local, stress-state-dependent failure criterion, permeability is incrementally increased to values of up to two orders of magnitude higher (Ingebritsen and Manning, 2010). As soon as overpressure is released, permeability returns to the background value given by the depth-dependent profile (Manning and Ingebritsen, 1999).

5.2. The hydrology of porphyry systems

With implementation of this dynamic permeability approach, the model can now describe the hydrology of porphyry copper systems and explain their characteristic fluid states (Fig. 7). The hydrothermal system self-organizes into a fluid plume with two distinct regions, separated by a hydrological divide (Weis and Driesner, 2013; Weis et al., 2012). The inner part is dominated by magmatic fluids under near-lithostatic pressures and temperatures above 500°C (Fig. 7A). The inferred ductile behavior at these high temperatures tends to decrease permeability, while the elevated fluid pressures keep interconnected pore space open or, in the case where fluid pressures exceed the near-lithostatic failure criterion, hydrofracture the rock. This mechanism creates fracturing-sealing cycles and the volatiles traverse this region in overpressure-permeability waves (Fig. 7B). Fluids are injected as single-phase fluids of intermediate density and phase-separate into vapor and brine upon ascent (Fig. 7A), in agreement with observations from fluid inclusions (e.g. Redmond et al., 2004; Williams-Jones and Heinrich, 2005).

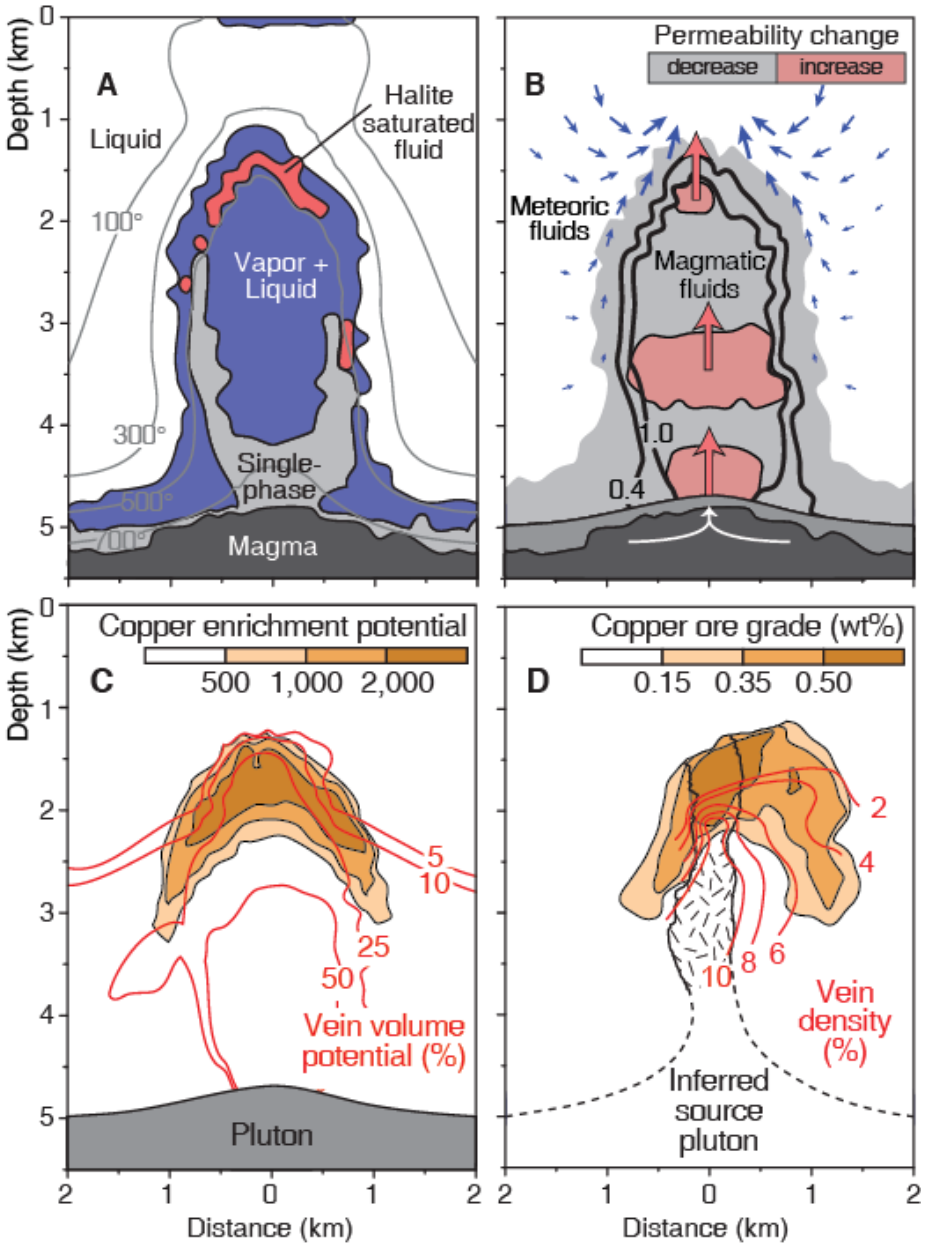

Fig. 7. Porphyry copper deposits are localized by focused flow of hot magmatic fluids that actively enhance rock permeability by hydraulic fracturing. This simulation (modified from Weis et al., 2012) shows that metal accumulation in porphyry ore shells is localised at a sharp pressure – temperature front, stabilized by the competing effects of permeability creation by magmatic fluid overpressure and permeability reduction resulting from magmatic heat advection. Figures show excerpts of 4 km width and 5.5. km depth from a modeling domain of 30 km width and 10 km depth, in which a large magma chamber forcefully expels saline magmatic fluid through a central cupola at 5 km depth. **A)** Distribution of fluid states and temperatures after 5000 years, with temperature contours in degrees Celsius (grey lines). **B)** Magmatic fluid injection through a cupola of the magma chamber establishes a hydrological divide separating an area dominated by magmatic fluid, near-lithosperic fluid presure and brittle/ductile rock behavior, from a permanently brittle domain dominated by convection of meteoric fluids. Solid black lines show the pore fluid factor (fluid pressure divided by lithostatic pressure): values lower than 0.4 indicate near-hydrostatic fluid pressure, while values around 1 indicate near-lithostatic fluid pressures. At 5000 years of simulation time, permeability changes are shown as deviations from the depth-dependent permeability profile characteristic of an average crust (as described in Manning and Ingebritsen, 1999). The magmatic fluids ascend in permeability waves representing repeated fracturin g-healing cycles. Schematic arrows illustrate flow of magmatic (red) and meteoric (grey) fluids. **C)** Copper enrichment potential (in relation to the concentration in the primary magmatic fluid) and vein volume potential are proxies calculated during the simulations and document the spatial distributions of veins in a deposit predicted by the numerical modeling. A copper enrichment potential of 1,000 relates to an upper limit of about 2. 5 wt% copper ore grade. **D)** Observed copper ore grade and vein density at the Bingham Canyon copper porphyry deposit (Gruen et al, 2010; Landtwing et al., 2005; Redmond et al., 2004).

The system is cooled by convection of surrounding meteoric fluids under near-hydrostatic conditions. The balance of heat supplied by magmatic volatiles and removed by meteoric waters stabilizes a sharp pressure-temperature front, describing the hydrological divide between areas of brittle and ductile rock behavior. Magmatic fluid pulses experience a sudden drop in both temperature and fluid pressure at this divide, which agrees with conditions inferred for porphyry mineralization. The model also predicts that fluids may saturate in solid halite at the hydrological divide (Fig. 7A). In contrast to the generalized pattern of salt water dynamics described previously, where halite precipitation triggered pulsating behavior (Fig. 2 and 3), the accumulated salt can be dissolved and flushed out immediately with the convection of meteoric water.

The accumulated amount of permeability increase can be scaled to a potential volume of vein quartz and used as a proxy for vein density (Weis et al., 2012). Assuming that copper is precipitated from the magmatic fluids within a temperature interval between 350°C and 450°C allows estimates of potential ore grades (Herzarkhani et al., 1999; Landtwing et al., 2005; Weis et al., 2012). The spatial distribution of predicted copper grades and vein densities are in good agreement with natural systems (Fig. 7C and D) (e.g. Arif and Baker, 2004; Dilles, 1987; Dilles and Einaudi, 1992; Gruen et al., 2010; Proffett, 2003).

5.3. Transition to epithermal systems

Porphyry deposits are inferred to be genetically linked to epithermal gold deposits (Richards, 2013; Sillitoe, 2010). Depending upon the geological setting, the two types of ore-forming systems can be telescoped, meaning that the tops of the porphyry systems are overprinted by the advanced argillic alteration often associated with high-sulfidation epithermal gold mineralization (Hedenquist and Lowenstern, 1994; Henley and Ellis, 1983; Izawa et al., 1990; Richards, 2013). Such a telescoped system develops in the numerical simulations of porphyry systems (Weis et al., 2012). Surges of magmatic fluids episodically cross the brittle-ductile transition and mix in variable proportions with the convecting ambient fluids. With these incoming pulses, the upflow zone fluctuates between a two-phase zone spanning the entire distance to the surface and a slightly cooler single-phase liquid state, with boiling limited to the uppermost part (as in Fig. 7A). Episodic boiling events have been inferred as a mechanism for gold precipitation in epithermal deposits, where mineralization is often concentrated in thin layers and associated with bladed calcite (Fournier, 1999; Izawa et al., 1990).

5.4. Temporal evolution and vein sequences

The initial phase of fluid expulsion is dominated by outward propagation of fluids (Fig. 8A), comparable to the general pattern in Fig. 1C. With continued degassing, the ascending magmatic fluids heat the surrounding rock to temperatures above the inferred brittle-ductile transition, which initiates the fracture-healing cycles between the magma body and the hydrologic divide. The changes in rock permeability also partially decouple the hydrological systems (blue and red arrows in Fig. 8B), which results in convection of meteoric waters cooling the system, and establishes the position of the temperature-pressure front (which is essentially a combination of the general patterns of Fig. 1B and Fig. 1D).

The early stages are dominated by the highest rates of volatile expulsion because the surface area of the cooling pluton is largest directly after emplacement. Fluid production has to be balanced by rapid movement of fluids away from the injection location, which can only be accommodated by permeability increases through intense hydraulic fracturing of the host rock. Consequently, the early stages experience the most intense veining and extend the brittle-ductile transition upward

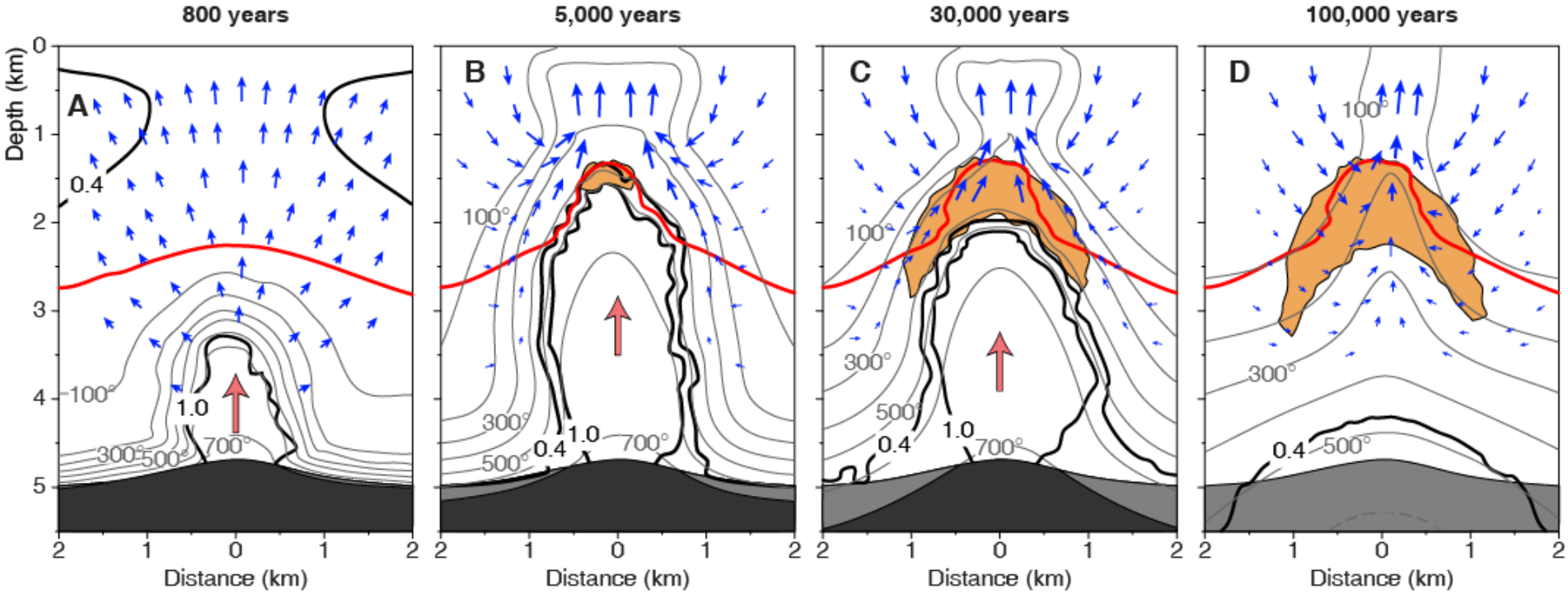

Fig. 8. Temporal evolution of a continental magmatic-hydrothermal system, simulating the initial pressure-buildup and quartz veining (**A**), the formation of a porphyry-style ore deposits during a period of self-stabilizing fluid pressure front while magma-chamber crystallization produces magmatic fluids (**B, C**), and the transition to thermal convection of hydrostatically-pressured meteoric water (**D**) (modified from Weis et al., 2012, 2013). Schematic arrows illustrate flow of magmatic (red) and meteoric (blue) fluids. The solid red line indicates the extent of intense veining due to hydraulic fracturing (vein volume potential of 10% as in Fig. 8C). The orange-colored field indicates the outline of a copper enrichment potential of 500 (Fig. 8C), which relates to an upper limit of about 1.25 wt% copper ore grade. Temperatures are given in degrees Celsius (grey lines). Solid black lines show the pore fluid factor. The gray tones at the base indicate the degree of crystallization of the magma chamber, distinguishing between areas above (dark gray) and below (light gray) the solidus temperature.

and outward. After 5,000 years of simulation time, most of the predicted vein density is already in place, while copper precipitation is just beginning with the establishment of the hydrological divide (Fig. 8B). These early stages represent intense stockwork veining and potassic alteration. Analyses of alteration halos in porphyry deposits also suggest that early quartz veining with related potassic alteration documents barren expulsion of magmatic fluids at the beginning of ore formation, pointing towards evene shorter time scales than modeled here (Cathles and Shannon, 2007).

With further inward crystallization, the surface area of the magma chamber gets smaller, resulting in a gradual decrease in the fluid source rate (illustrated by a retreat of the solid black lines (pore fluid factor) and the shrinking of the dark gray area at the base (magma chamber) in Fig. 8C). Fluid production can now be accommodated with less drastic permeability increases. Hence, the vein density increases only slightly during these later stages. The copper precipitation front slowly retreats to greater depths with the decreasing fluid source rate, meaning that copper is now precipitated in areas that had previously been dominated by the fracture-healing cycles at temperatures above the brittle-ductile transition. This evolution explains the vein sequence of intense (but barren) stockwork veining overprinted by later copper-bearing veins (cf. Gustafson and Hunt, 1975; Landtwing et al., 2005). The predicted mechanism for ore formation also explains why the ore shells have a sharp top coinciding with the highest vein density, while ore grades gradually fade out with greater depth (Sillitoe, 2010).

The process continues until all magmatic fluids have been released to the host rock (Fig. 8D), which takes about 50,000 to 100,000 years in these simulations. This time duration is in good agreement with recent geochronological studies of ore-forming events and previous modeling studies (Cathles, 1977; Driesner and Geiger, 2007; Hayba and Ingebritsen, 1997; Norton and Knight, 1977; von Quadt et al., 2011). The remaining heat of the pluton still drives convection of meteoric fluids that gradually mine the remnants of magmatic salt retained in the crust. This final stage may be related to late overprints of sodic alteration and can cause changes in the ore paragenesis or even redistribution of ore minerals (e.g. Dilles and Einaudi, 1992).

6. Discussion

The simulations have been kept generic in order to identify first-order controls on hydrothermal systems and their implications for ore formation. Model configurations have been constrained by geological observations and conceptual models. In turn, results from the quantitative numerical process modeling can be used to confirm or revise conceptual models, which may inspire further geological and hydrological observations.

6.1. Transient behavior of hydrothermal systems

Numerical simulations of volatile expulsion and salt water dynamics show that translating fluid-pressure estimates from fluid inclusions into paleodepth estimates can be difficult unless additional geological constraints are available (Fig.1 and 2). Significant variations in fluid pressure, exceeding a factor of three, have been observed in fluid inclusion studies at porphyry deposits (Ulrich et al., 2002). With far-field pressurization during initial phases of volatile expulsion, or pulsating fluid behavior related to halite precipitation and re-dissolution, fluid pressures deviate significantly from hydrostatic. The pressure field varies during the temporal and spatial evolution of the hydrothermal system. As a consequence, the degree of mixing of magmatic fluids with ambient fluids (meteoric fluids or seawater) depends on fluid source rate, permeability, and the stage of temporal evolution of the hydrothermal system. Further, salt water

dynamics that includes phase separation (which is almost inevitably the case at elevated temperatures) can be very complex. These hydrothermal systems may never reach a steady state, which makes them hard to assess with conceptual models alone and unresolvable for modeling approaches that rely on steady-state convection or use simplifying approximations for multi-phase flow or fluid properties.

6.2. Salt accumulation in hydrothermal systems

During extended periods of magmatic degassing, phase separation is likely to result in halite saturation, especially if high-enthalpy saline fluids reach shallower depths at near-hydrostatic conditions. Conceptual models should therefore also consider the amount of salt that might be retained in the crust by calculating mass and energy balances. Solid halite has been documented in very few magmatic-hydrothermal ore deposits (e.g. Muntean and Einaudi, 2000). However, the so-called halite trend observed in dense brine inclusions may indicate that solid halite was present at some stage of fluid evolution (Cloke and Kesler, 1979). The numerical simulations suggest that the presence of solid halite, at least temporarily, could be much more common than usually inferred.

6.3. Magma chamber dynamics

The actual mechanism of fluid extraction from a crystallizing magma chamber remains unexplored in the simulations. The simulations of porphyry copper systems describe the evolution of a hydrothermal system resulting from one-time emplacement of a large magma chamber. Field observations often indicate a more complex magmatic history, with several phases of magma emplacement of various compositions spanning geological periods considerably longer in duration than the main ore-forming event (Dilles, 1987; Sillitoe, 2010; Steinberger et al., 2013). Our simulations further assume that the rate of fluid production is proportional to the crystallization rate of the pluton, the second boiling scenario (Burnham and Ohmoto, 1980; Candela, 1991). However, convection within the magma chamber could result in faster fluid release at early stages. Fluids may also accumulate within the cupola of the magma chamber under an impermeable carapace and eject episodically, together with injections of porphyry dikes (e.g. Dilles, 1987). Modeling of fluid extraction from a magma chamber through diffusion of elements and advective transport within the magma chamber suggests that the efficiency of metal exsolution depends on the volatile contents and crystallinities of the mush (Huber et al., 2012).

6.4. Dynamic permeability

Similar to the permeability variations in our porphyry simulations, wave-like behavior of fluid transport through the crust has been described in a number of hydrogeological settings, enabling mass flux in areas of originally low permeability that may exceed the background flow regime by orders of magnitude. Solitary waves have been inferred to rapidly transfer fluids from an overpressured region at several kilometers depth to shallower levels along fault zones (Rice, 1992), in hydrocarbon reservoirs (Appold and Nunn, 2002; Joshi et al., 2012; Revil and Cathles, 2002), and within accretionary wedges (Bourlange and Henry, 2007). Fault-valve behavior describes fast fluid flow along faults triggered by earthquakes (Miller et al., 2004; Sibson, 1987) and is inferred for ore formation in mesothermal gold deposits (e.g. Sibson et al., 1988). Compaction-driven porosity waves have been described to be generated in metamorphic and sedimentary environments (Appold and Nunn, 2002; Connolly and Podlachikov, 1998). All of these processes have in common that they regard permeability and/or porosity as a dynamic

parameter of fluid-rock interaction, which may depend on tectonic setting, lithology, depth or fluid flow.

7. Ore Formation in Magmatic-Hydrothermal Systems

Chemistry-based classifications of ore deposits are important from a mining and exploration perspective and only indirectly refer to the physical driving forces for hydrothermal ore formation. Thermal convection, volatile expulsion and salt water dynamics are the three major components describing the physics of fluid flow, which in turn controls chemical enrichment in ore-forming magmatic-hydrothermal systems. The spatial and temporal combination of these processes is influenced by geological and tectonic settings. Size, depth and lifetime of the magma chamber control the style, extent, and duration of hydrothermal convection. The composition of the magma determines the amount of magmatic degassing. Regional and local stresses can influence the dynamic permeability of the crust. Permeability contrasts among different geological units and more localized fault zones can become first-order controls on the hydrology and provide mechanisms for ore precipitation. Permeability changes due to fracture-healing cycles under brittle or ductile rock behavior add transient dynamics. With increasing complexity, the three major components described in this paper can be identified as physical hydrological drivers for a number of ore deposit types.

7.1 Thermal convection and ore formation

Upper crustal magmatism induces buoyancy-driven fluid flow and can cause phase separation. Black smoker vent fields at mid-ocean ridge systems may serve as analogues for Cyprus-type VMS deposits (e.g. Solomon and Walshe, 1979). Convection of meteoric fluids in continental extensional settings can lead to low-sulfidation epithermal deposits such as the Madan Pb-Zn deposit (Kostova et al., 2004). In compressional settings, thermal convection of meteoric fluids with variable proportions of admixed magmatic fluids is inferred in porphyry copper systems and provides the link to epithermal gold deposits (Hedenquist and Lowenstern, 1994; Henley and Ellis, 1983; Richards, 2013; Sillitoe, 2010; Weis et al., 2012).

7.2. Volatile expulsion and ore formation

The hydrology of Cu-Mo-Au porphyry systems is characterized by high-pressure, high-temperature fluids of intermediate density that are expelled from an upper crustal magma chamber. These fluids separate into a low-salinity, low-density vapor and a high-salinity, high-density brine phase upon ascent. Field evidence and numerical modeling show that these systems form within a self-sealing, compressional regime at the transition from ductile to brittle rock behavior (e.g. Arif and Baker, 2004; Dilles, 1987; Gruen et al., 2010; Hedenquist et al., 1998; Weis et al., 2012).

Depending on the source rate, the hydrothermal conditions below volcanic fumaroles can range from strongly overpressured systems that may form hydrothermal breccias to vaporstatic pressure conditions. The hydrology is controlled by expansion of magmatic vapors, probably involves only minor components of ambient fluids, and might be accompanied by variable proportions of salt melts. These systems can cause advanced argillic alteration and are usually barren, except for porphyry Au deposits (e.g. Kodera et al., 2014).

Magmatic-hydrothermal systems can influence the regional hydrology over several kilometers, and magmatic volatiles may travel considerable distances to areas where the influence of magmatism is less obvious. Metamorphic devolatilization that leads to formation of orogenic gold

deposits follows similar hydrological principles in a different geological setting (Cox, 2005; Sibson et al., 1988). Carlin-type sediment-hosted deposits and so-called intermediate-sulfidation epithermal deposits are often inferred to be related to the expulsion of contracting fluids from a metamorphic or deep magmatic source (e.g. Muntean et al., 2011).

7.3. Salt water dynamics and ore formation

The addition of salt to an upper-crustal magmatic-hydrothermal system almost inevitably leads to phase separation and brine formation, both in submarine and subaerial environments. Heavy brines are not easily vented through the surface, which leads to accumulation of large amounts of salt within the crust during the most active stages of the fluid expulsion. This salt mass can later be brought to the surface by convection of ambient fluids in the waning stage. Brine mining is a common process in saline magmatic-hydrothermal systems and can be observed in the numerical simulations of mid-ocean ridges, submarine arc volcanoes, and porphyry systems. The NaCl-component can either be derived from seawater or from magmatic volatiles, which may also influence the metal budget associated with brine formation.

Brine mining in submarine systems may be related to the formation of Rosebery-type VMS deposits (e.g. Solomon and Walshe, 1979). In continental systems, brine mining may lead to typical Cordilleran polymetallic deposits (e.g. Catchpole et al., 2011). Brine mining is less pronounced in the simulations of porphyry copper systems because the interplay of fluid flow and dynamic permeability results in brine transport under high pressure gradients to relatively shallow depths, where it can be diluted immediately and transported to the surface by the convecting meteoric fluids.

8. Conclusions

Numerical simulation of hydrothermal ore-forming processes is a powerful tool for quantifying the governing mass, solute, and heat fluxes and to test geological interpretations, but may also lead to intuitively unexpected results. Understanding the physical driving forces controlling the formation of characteristic mineral assemblages and alteration sequences can improve our conceptual models of ore formation and might eventually assist in conceptual exploration targeting. The simulated hydrothermal phenomena resulting from nonlinear properties of fluids and rocks identify four somewhat counterintuitive relations that are of interest for ore-forming processes and call for further geological or analytical investigation:

(1) In mid-ocean ridge hydrothermal systems, focused downflow of warm fluids surrounding hot upflow zones provides an efficient mechanism for metal leaching from the new ocean crust and subsequent formation of massive sulfide deposits.

(2) Phase separation in submarine and subaerial magmatic-hydrothermal systems may lead to spatially and temporally distinct venting behavior and ore formation of metals preferentially fractionating into a S-rich vapor or a Cl-rich brine phase.

(3) Salt from magmatic brines are likely to accumulate in the crust, and can only be mobilized by dilution resulting from convective meteoric circulation.

(4) Porphyry copper ore shells are predicted to be localized at a hydrological front related to a relatively abrupt transition from brittle to ductile rock behavior. The modeled precipitation mechanism introduces an essential role for thermal convection of ambient fluids in cooling the areas dominated by volatile expulsion. The gradual retreat of this divide to greater depths

explains the geological relationship of copper-bearing veins cutting barren stockwork veins. The hydrological divide can also explain the transition to epithermal deposits where magmatic and meteoric fluids mix on ascent to the surface. Even though the focus of this paper is on magmatic-hydrothermal ore system, hydrodynamic analysis also pertains to orogenic ore systems whose metamorphic source region is overpressured, and to near-hydrostatically pressured sediment-hosted ore systems that are more directly influenced by surface processes.

Acknowledgments

Many thanks to Steven Ingebritsen and Martin Appold for their very helpful reviews, to Karen D. Kelley for her editorial comments and to Christoph A. Heinrich for helpful comments on earlier versions of the manuscript. The work has been supported by the Swiss National Science Foundation within various funding periods.

Appendix

Governing Equations

Subsurface fluid flow in porous and fractured media can be described by Darcy's law (Ingebritsen et al., 2006). The classical groundwater formulation calculates the fluid flux through porous rocks by determining the hydraulic head, which describes the different heights of interconnected water columns. For the description of hydrothermal systems that are characterized by non-linear fluid properties, Darcy's law for a single-phase fluid is more conveniently formulated as

$$v = -\frac{k}{\mu}\left(\nabla p - \rho g\right), \tag{1}$$

with the Darcy velocity v, the permeability k, the fluid viscosity μ, the fluid pressure p, the fluid density ρ and the acceleration due to gravity g. The Darcy velocity describes a volume flux of fluid across an area perpendicular to flow with units of $m^3\ m^{-2}\ s^{-1}$. The pore velocity represents the volumetric flux per unit cross sectional area of the actual pore space as

$$v_{pore} = \frac{v}{\phi}, \tag{2}$$

with the effective porosity ϕ, which has a value between 0 (no pore space) and 1 (pore space only), resulting in $v_{pore} \geq v$. Permeability and porosity are related variables but describe different properties of the rock. The relation of permeability and porosity is not straightforward and strongly depends on the type, texture and structure of the rock formation.

Evaluating fluid flow by Darcy's law with conceptual, analytical or numerical models requires that the system can be approximated with so-called representative elementary volumes (REV), where values for permeability and porosity can be regarded as constant. Within the REV concept, fractured media can also be described with a continuum, porous medium approach. Fracture zones can be described by regions of high permeability within the domain. The term $\frac{k}{\mu}$ in Darcy's law (1) then describes the resistance to flow and the relation implies that increasing fluid viscosity μ by an order of magnitude, e.g. heating water from 10 to 200°C, has the same effect as increasing rock permeability by an order of magnitude.

The driving force for Darcy flux is the deviation of the gradient in fluid pressure from the gravitational load of the fluid column, $\nabla p - \rho g$. High permeability zones are only relevant for the hydrothermal system in the presence of a driving force.

Conservation equations for single-phase flow

To understand and characterize a hydrothermal system, the flow system has to be evaluated for the entire domain by formulating the continuity equation of mass conservation

$$\begin{aligned}\frac{\partial(\phi\rho)}{\partial t} &= -\nabla\cdot(v\rho)+Q \\ &= \nabla\cdot\left(\frac{k}{\mu}(\nabla p-\rho g)\rho\right)+Q\end{aligned}, \tag{3}$$

where Q describes a source or sink of fluid mass, e.g. by injecting or withdrawing fluid. The temporal change in stored fluid mass $(\phi\rho)$ is balanced by the inflow and the outflow, and buoyancy-driven convection can now be maintained by imposing a horizontal pressure gradient, $\nabla p_{horizontal} \neq 0$, from a colder high-density region to a hotter low-density region. This horizontal pressure gradient results in

$$\nabla p_{vertical}^{downflow} < \rho_{cold} g\,, \tag{4}$$

and

$$\nabla p_{vertical}^{upflow} > \rho_{hot} g\,. \tag{5}$$

In the presence of large source terms Q, such as during rapid magmatic degassing, the rate of fluid injection has to be balanced by the mass flux away from the source.

Solutes in the fluids can be transported as

$$\frac{\partial(\phi\rho X)}{\partial t} = -\nabla\cdot(v\rho X)+\nabla\cdot\left(D\nabla(\rho X)\right)+Q_s\,, \tag{6}$$

with the mass fraction of the solute X, a dispersion coefficient D, and a source term Q_s.

The heat imposed by the magma can be transmitted by conduction through the rock as

$$\begin{aligned}(1-\phi)\frac{\partial H_r}{\partial t} &= (1-\phi)c_{pr}\rho_r\frac{\partial T}{\partial t} \\ &= \nabla\cdot(K\nabla T)+Q_c\end{aligned}, \tag{7}$$

with the index r indicating the rock, the enthalpy H, the heat capacity c_p, the temperature T, the thermal conductivity K, and a heat source term Q_c, as well as through advection by the fluid as

$$\begin{aligned}\phi\frac{\partial H_f}{\partial t} &= \phi\frac{\partial(\rho_f h_f)}{\partial t} \\ &= -\nabla\cdot(v\rho_f h_f)+Q_a\end{aligned}, \tag{8}$$

with the index f indicating the fluid, the specific enthalpy h, and a source term Q_a, that accounts for the energy added or subtracted by a fluid source or sink.

Heat conduction and advection have distinctly different profiles for heat propagation and act on different time-scales, mainly depending on the permeability, k, which can vary over many orders

of magnitude. In magmatic-hydrothermal systems we can assume that porosity ϕ normally has small values and that flow rates are slow enough that fluid and rock are in local thermal equilibrium, that is

$$H_t = \phi H_f + (1-\phi) H_r \tag{9}$$

is conserved in the combined advection-diffusion equation

$$\frac{\partial H_t}{\partial t} = \nabla \cdot (K \nabla T) + Q_c - \nabla \cdot (v \rho_f h_f) + Q_a . \tag{10}$$

This local thermal equilibrium results in a decoupled propagation of solute and thermal fronts. If hot magmatic fluids propagate into colder rock units, heat is rapidly lost to the rock mass, while solutes can be transported further (unless the solubility of the component drops drastically with temperature). On the other hand, once a steady flux of magmatic volatiles has heated the host rock, fluids may ascend through the crust with little loss of energy to the surroundings, and temperature changes being limited to abiabatic effects.

Multi-component, multi-phase flow

Two-phase fluid flow of pure water can be described by an extended form of Darcy's law (1) as

$$v_i = -k \frac{k_{ri}}{\mu} (\nabla p - \rho_i g) \qquad i = \{v, l\}, \tag{11}$$

with the index i indicating the fluid phases vapor v and liquid l, and the relative permeability k_r of the phase indicated (Ingebritsen et al., 2006). Relative permeability models account for the two (or more) fluid phases competing for the available permeability and are usually formulated in terms of dependence on the volumetric saturation S of the respective phase. Linear relative permeability models, where individual values of k_{ri} add up to 1, are commonly applied for high-temperature fracture-dominated systems (cf. Ingebritsen et al., 2010). Residual saturations determine the minimum saturation for flow, e.g. if the volumetric saturation of the liquid phase falls below its residual saturation, the phase is only present as a wetting phase in the pore space, with too little connectivity between patches of the liquid to ensure flow. Residual saturations incorporate some capillary effects, which are otherwise commonly not calculated explicitly for simulations of high-temperature systems, due to a lack of empirical data and the fact that surface tension of water decreases with temperature (Ingebritsen et al., 2010). The simulations presented in this paper use a residual saturation for the liquid phase of $R_l = 0.3 \cdot (1 - S_h)$, with the index h for halite, $R_v = 0.0$ for the vapor phase, and $k_{rl} + k_{rv} = 1 - S_h$. The latter relation infers that the accumulation of solid halite reduces the pore space and permeability that is available for the mobile phases liquid and vapor.

Adding further components like NaCl or CO_2 to the systems, the conservation equations (3), (6) and (10) for a system with n possible mobile fluid phases and m possible immobile (solid) phases can be formulated as

$$\frac{\partial\left(\phi\sum_{i=1}^{n+m}S_i\rho_i\right)}{\partial t}=-\sum_{i=1}^{n}\nabla\cdot\left(v_i\rho_i\right)+Q\,, \tag{12}$$

for the conservation of mass,

$$\frac{\partial\left(\phi\sum_{i=1}^{n+m}S_i\rho_iX_i\right)}{\partial t}=-\sum_{i=1}^{n}\nabla\cdot\left(v_i\rho_iX_i\right)+\sum_{i=1}^{n}\nabla\cdot\left(D\nabla\left(\rho_iX_i\right)\right)+Q_s\,, \tag{13}$$

for the conservation of a solute s, and

$$\frac{\partial\left(\left(1-\phi\right)\rho_rh_r+\phi\sum_{i=1}^{n+m}S_i\rho_ih_i\right)}{\partial t}=\nabla\cdot\left(K\nabla T\right)+Q_c-\sum_{i=1}^{n}\nabla\cdot\left(v_i\rho_ih_i\right)+Q_a\,, \tag{14}$$

for the conservation of energy.

Multi-phase flow of multi-component fluids requires that an accurate thermodynamic model for fluid properties and phase relations exists and is implemented into the numerical model.

References

Alt, J.C., 1995, Sulfur isotopic profile through the oceanic-crust - sulfur mobility and seawater-crustal sulfur exchange during hydrothermal alteration: Geology, v. 23, p. 585-588.

Appold, M.S., and Nunn, J.A., 2002, Numerical models of petroleum migration via buoyancy-driven porosity waves in viscously deformable sediments: Geofluids, v. 2, p. 233-247.

Arif, J., and Baker, T., 2004, Gold paragenesis and chemistry at Batu Hijau, Indonesia: implications for gold-rich porphyry copper deposits: Mineralium Deposita, v. 39, p. 523-535.

Baker, E.T., and Urabe, T., 1996, Extensive distribution of hydrothermal plumes along the superfast spreading East Pacific Rise, 13 degrees 30'-18 degrees 40'S: Journal of Geophysical Research-Solid Earth, v. 101, p. 8685-8695.

Bani-Hassan, N., Iyer, K., Rupke, L.H., and Borgia, A., 2012, Controls of bathymetric relief on hydrothermal fluid flow at mid-ocean ridges: Geochemistry Geophysics Geosystems, v. 13, Q05002.

Bourlange, S., and Henry, P., 2007, Numerical model of fluid pressure solitary wave propagation along the decollement of an accretionary wedge: application to the Nankai wedge: Geofluids, v. 7, p. 323-334.

Burnham, C.W., and Ohmoto, H., 1980, Late-stage processes of felsic magmatism: Mining Geology Special Issue, p. 1-11.

Butterfield, D.A., Massoth, G.J., McDuff, R.E., Lupton, J.E., and Lilley, M.D., 1990, Geochemistry of hydrothermal fluids from Axial Seamount hydrothermal emissions study vent field, Juan-de-Fuca Ridge: subseafloor boiling and subsequent fluid-rock interaction: Journal of Geophysical Research-Solid Earth and Planets, v. 95, p. 12895-12921.

Butterfield, D.A., McDuff, R.E., Mottl, M.J., Lilley, M.D., Lupton, J.E., and Massoth, G.J., 1994, Gradients in the composition of hydrothermal fluids from the Endeavor segment vent field - phase-separation and brine loss: Journal of Geophysical Research-Solid Earth, v. 99, p. 9561-9583.

Candela, P.A., 1991, Physics of aqueous phase evolution in plutonic environments: American Mineralogist, v. 76, p. 1081-1091.

Catchpole, H., Kouzmanov, K., Fontbote, L., Guillong, M., and Heinrich, C.A., 2011, Fluid evolution in zoned Cordilleran polymetallic veins - Insights from microthermometry and LA-ICP-MS of fluid inclusions: Chemical Geology, v. 281, p. 293-304.

Cathles, L.M., 1977, An analysis of the cooling of intrusives by ground-water convection which includes boiling: Economic Geology, v. 72, p. 804-826.

Cathles, L.M., and Shannon, R., 2007, How potassium silicate alteration suggests the formation of porphyry ore deposits begins with the nearly explosive but barren expulsion of large volumes of magmatic water: Earth and Planetary Science Letters, v. 262, p. 92-108.

Charlou, J.L., Fouquet, Y., Donval, J.P., Auzende, J.M., JeanBaptiste, P., Stievenard, M., and Michel, S., 1996, Mineral and gas chemistry of hydrothermal fluids on an ultrafast spreading ridge: East Pacific Rise, 17 degrees to 19 degrees S (Naudur cruise, 1993) phase separation processes

controlled by volcanic and tectonic activity: Journal of Geophysical Research-Solid Earth, v. 101, p. 15899-15919.

Chiba, H., Masuda, H., Lee, S.Y., and Fujioka, K., 2001, Chemistry of hydrothermal fluids at the TAG active mound, MAR 26 degrees N, in 1998: Geophysical Research Letters, v. 28, p. 2919-2922.

Cloke, P.L., and Kesler, S.E., 1979, Halite trend in hydrothermal solutions: Economic Geology, v. 74, p. 1823-1831.

Connolly, J.A.D., and Podladchikov, Y.Y., 1998, Compaction-driven fluid flow in viscoelastic rock: Geodinamica Acta, v. 11, p. 55-84.

Coumou, D., Driesner, T., and Heinrich, C.A., 2008, The structure and dynamics of mid-ocean ridge hydrothermal systems: Science, v. 321, p. 1825-1828.

Coumou, D., Driesner, T., Geiger, S., Paluszny, A., and Heinrich, C.A., 2009a, High-resolution three-dimensional simulations of mid-ocean ridge hydrothermal systems: Journal of Geophysical Research-Solid Earth, v. 114, B03212.

Coumou, D., Driesner, T., Weis, P., and Heinrich, C.A., 2009b, Phase separation, brine formation, and salinity variation at Black Smoker hydrothermal systems: Journal of Geophysical Research-Solid Earth, v. 114, p. B03212.

Cox, S.F., 2005, Coupling between deformation, fluid pressures, and fluid flow in ore-producing hydrothermal systems at depth in the crust: Economic Geology 100th Anniversary Volume, p. 39-75.

Cox, S.F., 2010, The application of failure mode diagrams for exploring the roles of fluid pressure and stress states in controlling styles of fracture-controlled permeability enhancement in faults and shear zones: Geofluids, v. 10, p. 217-233.

de Ronde, C.E.J., Hannington, M.D., Stoffers, P., Wright, I.C., Ditchburn, R.G., Reyes, A.G., Baker, E.T., Massoth, G.J., Lupton, J.E., Walker, S.L., Greene, R.R., Soong, C.W.R., Ishibashi, J., Lebon, G.T., Bray, C.J., and Resing, J.A., 2005, Evolution of a submarine magmatic-hydrothermal system: Brothers volcano, southern Kermadec arc, New Zealand: Economic Geology, v. 100, p. 1097-1133.

Dilles, J.H., 1987, Petrology of the Yerington Batholith, Nevada - Evidence for evolution of porphyry copper ore fluids: Economic Geology, v. 82, p. 1750-1789.

Dilles, J.H., and Einaudi, M.T., 1992, Wall-rock alteration and hydrothermal flow paths about the Ann-Mason porphyry copper deposit, Nevada - a 6 km vertical reconstruction: Economic Geology, v. 87, p. 1963-2001.

Driesner, T., 2007, The system H2O-NaCl. Part II: Correlations for molar volume, enthalpy, and isobaric heat capacity from 0 to 1000 degrees C, 1 to 5000 bar, and 0 to 1 X-NaCl: Geochimica et Cosmochimica Acta, v. 71, p. 4902-4919.

Driesner, T., and Geiger, S., 2007, Numerical simulation of multiphase fluid flow in hydrothermal systems, *in* Liebscher, A., and Heinrich, C. A., eds., Fluid-Fluid Interactions, 65. Reviews in Mineralogy & Geochemistry: Chantilly, Mineralogical Soc Amer, p. 187-212.

Driesner, T., and Heinrich, C.A., 2007, The system H2O-NaCl. Part I: Correlation formulae for phase relations in temperature-pressure-composition space from 0 to 1000 degrees C, 0 to 5000 bar, and 0 to 1 X-NaCl: Geochimica et Cosmochimica Acta, v. 71, p. 4880-4901.

Edmonds, H.N., German, C.R., Green, D.R.H., Huh, Y., Gamo, T., and Edmond, J.M., 1996, Continuation of the hydrothermal fluid chemistry time series at TAG, and the effects of ODP drilling: Geophysical Research Letters, v. 23, p. 3487-3489.

Fournier, R.O., 1999, Hydrothermal processes related to movement of fluid from plastic into brittle rock in the magmatic-epithermal environment: Economic Geology, v. 94, p. 1193-1211.

Foustoukos, D.I., and Seyfried, W.E., 2007, Fluid phase separation processes in submarine hydrothermal systems, *in* Liebscher, A., and Heinrich, C.A., eds., Fluid-Fluid Interactions, 65. Reviews in Mineralogy and Geochemistry, Mineralogical Society of America, Geochemical Society, p. 213-239.

Gallant, R.M., and Von Damm, K.L., 2006, Geochemical controls on hydrothermal fluids from the Kairei and Edmond Vent Fields, 23 degrees-25 degrees S, Central Indian Ridge: Geochemistry Geophysics Geosystems, v. 7, Q06018.

Geiger, S., Robert, S., Matthai, S.K., Zoppou, C., and Burri, A., 2004, Combining finite element and finite volume methods for efficient multiphase flow simulations in highly heterogeneous and structurally complex geologic media: Geofluids, v. 4, p. 284-299.

Ginster, U., Mottl, M.J., and Vonherzen, R.P., 1994, Heat-flux from black smokers on the Endeavor and Cleft segments, Juan-de-Fuca Ridge: Journal of Geophysical Research-Solid Earth, v. 99, p. 4937-4950.

Glickson, D.A., Kelley, D.S., and Delaney, J.R., 2007, Geology and hydrothermal evolution of the Mothra Hydrothermal Field, Endeavour Segment, Juan de Fuca Ridge: Geochemistry Geophysics Geosystems, v. 8, Q06010.

Gruen, G., 2011, Subsurface hydrology of submarine arc volcanoes, with application to the active hydrothermal system at Brothers volcano, Kermadec arc, New Zealand: Unpublished PhD thesis, ETH Zurich, 99 p.

Gruen, G., Heinrich, C.A., and Schroeder, K., 2010, The Bingham Canyon porphyry Cu-Mo-Au deposit. II. Vein geometry and ore shell formation by pressure-driven rock extension: Economic Geology, v. 105, p. 69-90.

Gruen, G., Weis, P., Driesner, T., de Ronde, C.E.J., and Heinrich, C.A., 2012, Fluid-flow patterns at Brothers Volcano, Southern Kermadec Arc: Insights from geologically constrained numerical simulations: Economic Geology, v. 107, p. 1595-1611.

Gunnarsson, G., Arnaldsson, A., and Oddsdottir, A.L., 2011, Model Simulations of the Hengill Area, Southwestern Iceland: Transport in Porous Media, v. 90, p. 3-22.

Gustafson, L.B., and Hunt, J.P., 1975, Porphyry copper-deposit at El Salvador, Chile: Economic Geology, v. 70, p. 857-912.

Haar, L., Gallagher, J.S., and Kell, G.S., 1984, NBS/NRC Steam Tables: Thermodynamic and transport properties and computer programs for vapor and liquid states of water in SI units: Hemisphere Publishing Corporation, Washington, New York,London, pp. 320.

Halbach, P., Tunnicliffe, V., and Hein, J.R., 2003, Energy and Mass Transfer in Marine Hydrothermal Systems: Berlin, Dahlem University Press, pp. 365.

Hannington, M.D., 2014, Volcanogenic massive sulfide deposits, *in* Holland, H. D., and Turekian, K. K., eds., Treatise on Geochemistry: The Geochemistry of Ore Deposits, 28: Oxford, Elsevier-Pergamon, p. 463-488.

Hannington, M., Jamieson, J., Monecke, T., Petersen, S., and Beaulieu, S., 2011, The abundance of seafloor massive sulfide deposits: Geology, v. 39, p. 1155-1158.

Hanson, R.B., 1995, The hydrodynamics of contact-metamorphism: Geological Society of America Bulletin, v. 107, p. 595-611.

Hayba, D.O., and Ingebritsen, S.E., 1997, Multiphase groundwater flow near cooling plutons: Journal of Geophysical Research, v. 102, p. 12235-12252.

Hedenquist, J.W., and Lowenstern, J.B., 1994, The role of magmas in the formation of hydrothermal ore deposits: Nature, v. 370, p. 519-527.

Hedenquist, J.W., Arribas, A., and Reynolds, T.J., 1998, Evolution of an intrusion-centered hydrothermal system: Far Southeast-Lepanto porphyry and epithermal Cu-Au deposits, Philippines: Economic Geology, v. 93, p. 373-404.

Heinrich, C.A., and Candela, P.A., 2014, Fluids and ore formation in the Earth's crust, *in* Holland, H.D., and Turekian, K.K., eds., Treatise on Geochemistry: The Geochemistry of Ore Deposits, 28: Oxford, Elsevier-Pergamon, p. 1-28.

Heinrich, C.A., Günther, D., Audétat, A., Ulrich, T., and Frischknecht, R., 1999, Metal fractionation between magmatic brine and vapor, determined by microanalysis of fluid inclusions: Geology, v. 27, p. 755-758.

Hemley, J.J., Cygan, G.L., Fein, J.B., Robinson, G.R., and Dangelo, W.M., 1992, Hydrothermal ore-forming processes in the light of studies in rock-buffered systems. 1. Iron-copper-zinc-lead sulfide solubility relations: Economic Geology, , v. 87, p. 1-22.

Henley, R.W., and Ellis, A.J., 1983, Geothermal systems ancient and modern - a geochemical review: Earth-Science Reviews, v. 19, p. 1-50.

Henley, R.W., and McNabb, A., 1978, Magmatic vapor plumes and groundwater interaction in porphyry copper emplacement: Economic Geology, v. 73, p. 1-20.

Herzarkhani, A., Williams-Jones, A.E., and Gammons, C.H., 1999, Factors controlling copper solubility and chalcopyrite deposition in the Sungun porphyry copper deposit, Iran: Mineralium Deposita, v. 34, p. 770-783.

Huber, C., Bachmann, O., Vigneresse, J.L., Dufek, J., and Parmigiani, A., 2012, A physical model for metal extraction and transport in shallow magmatic systems: Geochemistry Geophysics Geosystems, v. 13, Q08003.

Ingebritsen, S.E., and Appold, M.S., 2012, The physical hydrogeology of ore deposits: Economic Geology, v. 107, p. 559-584.

Ingebritsen, S.E., Sanford, S., and Neuzil, C., 2006, Groundwater in Geologic Processes, 2nd ed., Cambridge University Press, 536 p.

Ingebritsen, S.E., Geiger, S., Hurwitz, S., and Driesner, T., 2010, Numerical Simulation of Magmatic Hydrothermal Systems: Reviews of Geophysics, v. 48, RG1002.

Izawa, E., Urashima, Y., Ibaraki, K., Suzuki, R., Yokoyama, T., Kawasaki, K., Koga, A., and Taguchi, S., 1990, The Hishikari gold deposit - high-grade epithermal veins in Quaternary volcanics of Southern Kyushu, Japan: Journal of Geochemical Exploration, v. 36, p. 1-56.

James, R.H., Elderfield, H., and Palmer, M.R., 1995, The chemistry of hydrothermal fluids from the Broken Spur site, 29-degrees-N Mid-Atlantic Ridge: Geochimica et Cosmochimica Acta, v. 59, p. 651-659.

Johnson, H.P., Becker, K., and Vonherzen, R., 1993, Near-axis heat-flow measurements on the northern Juan-de-Fuca Ridge - Iimplications for fluid ciculation in oceanic crust: Geophysical Research Letters, v. 20, p. 1875-1878.

Joshi, A., Appold, M.S., and Nunn, J.A., 2012, Evaluation of solitary waves as a mechanism for oil transport in poroelastic media: A case study of the South Eugene Island field, Gulf of Mexico basin: Marine and Petroleum Geology, v. 37, p. 53-69.

Jupp, T., and Schultz, A., 2000, A thermodynamic explanation for black smoker temperatures: Nature, v. 403, p. 880-883.

Keating, G.N., Geissman, J.W., and Zyvoloski, G.A., 2002, Multiphase modeling of contact metamorphic systems and application to transitional geomagnetic fields: Earth and Planetary Science Letters, v. 198, p. 429-448.

Kesler, S.E., 1994, Mineral resources, economics and the environment: New York, McMillan, 391 p.

Kipp Jr., K.L., Hsieh, P.A., and Charlton, S.R., 2008, Guide to the Revised Ground-Water Flow and Heat Transport Simulator: HYDROTHERM -- Version 3: U. S. Geological Survey, Techniques and Methods, 6-A25, 160 p.

Kissling, W.M., 2005, Transport of three-phase hyper-saline brines in porous media: Theory and code implementation: Transport in Porous Media, v. 61, p. 25-44.

Kodera, P., Heinrich, C.A., Walle, M., and Lexa, J., 2014, Magmatic salt melt and vapor: Extreme fl uids forming porphyry gold deposits in shallow subvolcanic settings: Geology, doi:10.1130/G35270.1.

Kostova, B., Pettke, T., Driesner, T., Petrov, P., and Heinrich, C.A., 2004, LA ICP-MS study of fluid inclusions in quartz from the Yuzhna Petrovitsa deposit, Madan ore field, Bulgaria: Schweizerische Mineralogische und Petrographische Mitteilungen, v. 84, p. 25-36.

Landtwing, M.R., Pettke, T., Halter, W.E., Heinrich, C.A., Redmond, P.B., Einaudi, M.T., and Kunze, K., 2005, Copper deposition during quartz dissolution by cooling magmatic-hydrothermal fluids: The Bingham porphyry: Earth and Planetary Science Letters, v. 235, p. 229-243.

Lewis, K.C., and Lowell, R.P., 2009, Numerical modeling of two-phase flow in the NaCl-H2O system: Introduction of a numerical method and benchmarking: Journal of Geophysical Research-Solid Earth, v. 114, B05202.

Lowell, R.P., Rona, P.A., and Von Herzen, R.P., 1995, Sear-floor hydrothermal systems: Journal of Geophysical Research-Solid Earth, v. 100, p. 327-352.

Manning, C.E., and Ingebritsen, S.E., 1999, Permeability of the continental crust: Implications of geothermal data and metamorphic systems: Reviews of Geophysics, v. 37, p. 127-150.

Massoth, G.J., Butterfield, D.A., Lupton, J.E., McDuff, R.E., Lilley, M.D., and Jonasson, I.R., 1989, Submarine venting of phase-separated hydrothermal fluids at Axial Vocano, Juan-de-Fuca Ridge: Nature, v. 340, p. 702-705.

Matthai, S.K., Geiger, S., Roberts, S.G., Paluszny, A., Belayneh, M., Burri, A., Mezentsev, A., Lu, H., Coumou, D., Driesner, T., and Heinrich, C.A., 2007, Numerical simulation of multi-phase fluid flow in structurally complex reservoirs, *in* Jolley, S.J., Barr, D., Walsh, J.J., and Knipe, R.J., eds., Structurally Complex Reserviors, 292. Geological Society Special Publication: London, The Geological Society, p. 405-429.

McCuaig, T.C., and Kerrich, R., 1998, P—T—t—deformation—fluid characteristics of lode gold deposits: evidence from alteration systematics: Ore Geology Reviews, v. 12, p. 381-453.

Miller, S.A., Collettini, C., Chiaraluce, L., Cocco, M., Barchi, M., and Kaus, B.J.P., 2004, Aftershocks driven by a high-pressure CO2 source at depth: Nature, v. 427, p. 724-727.

Muntean, J.L., and Einaudi, M.T., 2000, Porphyry gold deposits of the Refugio district, Maricunga belt, northern Chile: Economic Geology, v. 95, p. 1445-1472.

Muntean, J.L., Cline, J.S., Simon, A.C., and Longo, A.A., 2011, Magmatic-hydrothermal origin of Nevada's Carlin-type gold deposits: Nature Geoscience, v. 4, p. 122-127.

Norton, D., and Knight, J., 1977, Transport phenomena in hydrothermal systems: Cooling plutons: American Journal of Science, v. 277, p. 937-981.

Oosting, S.E., and Von Damm, K.L., 1996, Bromide/chloride fractionation in seafloor hydrothermal fluids from 9-10 degrees N east Pacific rise: Earth and Planetary Science Letters, v. 144, p. 133-145.

Pokrovski, G.S., Borisova, A.Y., and Harrichoury, J.C., 2008, The effect of sulfur on vapor-liquid fractionation of metals in hydrothermal systems: Earth and Planetary Science Letters, v. 266, p. 345-362.

Proffett, J.M., 2003, Geology of the Bajo de la Alumbrera porphyry copper-gold deposit, Argentina: Economic Geology, v. 98, p. 1535-1574.

Pruess, K., 2004, The TOUGH codes - A family of simulation tools for multiphase flow and transport processes in permeable media: Vadose Zone Journal, v. 3, p. 738-746.

Ramondenc, P., Leonid, N.G.A., Von Damm, K.L., and Lowell, R.P., 2006, The first measurements of hydrothermal heat output at 9 degrees 50 ' N, East Pacific Rise: Earth and Planetary Science Letters, v. 245, p. 487-497.

Redmond, P.B., Einaudi, M.T., Inan, E.E., Landtwing, M.R., and Heinrich, C.A., 2004, Copper deposition by fluid cooling in intrusion-centered systems: New insights from the Bingham porphyry ore deposit, Utah: Geology, v. 32, p. 217-220.

Revil, A., and Cathles, L.M., 2002, Fluid transport by solitary waves along growing faults - A field example from the South Eugene Island Basin, Gulf of Mexico: Earth and Planetary Science Letters, v. 202, p. 321-335.

Rice, J. R., 1992, Fault stress states, pore pressure distributions, and the weakness of the San Andreas Faultpp, *in* Evans, B., Wong, T.F., ed., Fault Mechanics and Transport Properties of Rocks, 51. Int. Geophys. Series, Academic, New York, p. 475–475.

Richards, J.P., 2013, Giant ore deposits formed by optimal alignments and combinations of geological processes: Nature Geoscience, v. 6, p. 911-916.

Sammel, E.A., Ingebritsen, S.E., and Mariner, R.H., 1988, The hydrothermal system at Newberry Volcano, Oregon: Journal of Geophysical Research-Solid Earth and Planets, v. 93, p. 10149-10162.

Seyfried, W.E., and Ding, K., 1995, Phase equilibria in subseafloor hydrothermal Systems: a review of the role of redox, temperature, pH and dissolved Cl on the chemistry of hot spring fluids at mid-ocean ridges, *in* Humphris, S.E., Zierenberg, R.A., Mullineaux, L.S., and Thomson, R.E., eds., Seafloor Hydrothermal Systems: Physical, Chemical, Biological, and Geological Interactions, 91. Geophysical Monograph, American Geophysical Union, p. 248-272.

Seyfried, W.E., Seewald, J.S., Berndt, M.E., Ding, K., and Foustoukos, D.I., 2003, Chemistry of hydrothermal vent fluids from the Main Endeavour Field, northern Juan de Fuca Ridge: Geochemical controls in the aftermath of June 1999 seismic events: Journal of Geophysical Research-Solid Earth, v. 108.

Sibson, R.H., 1987, Earthquake rupturing as a mineralizing agent in hydrothermal systems: Geology, v. 15, p. 701-704.

Sibson, R.H., Robert, F., and Poulsen, K.H., 1988, High-angle reverse faults, fluid-pressure cycling, and mesothermal gold-quartz deposits: Geology, v. 16, p. 551-555.

Sillitoe, R.H., 2010, Porphyry copper systems: Economic Geology, v. 105, p. 3-41.

Solomon, M., and Walshe, J.L., 1979, Formation of massive sulfide deposits on the sea floor: Economic Geology, v. 74, p. 797-813.

Solomon, M., Tornos, F., Large, R.R., Badham, J.N.P., Both, R.A., and Zaw, K., 2004, Zn-Pb-Cu volcanic-hosted massive sulphide deposits: Criteria for distinguishing brine pool-type from black smoker-type sulphide deposition: Ore Geology Reviews, v. 25, p. 259-283.

Steinberger, I., Hinks, D., Driesner, T., and Heinrich, C.A., 2013, Source plutons driving porphyry copper ore formation: Combining geomagnetic data, thermal constraints, and chemical mass balance to quantify the magma chamber beneath the Bingham Canyon deposit: Economic Geology, v. 108, p. 605-624.

Ulrich, T., Günther, D., and Heinrich, C.A., 2002, The evolution of a porphyry Cu-Au deposit, based on LA-ICP-MS analysis of fluid inclusions: Bajo de la Alumbrera: Economic Geology, v. 97, p. 1365-1372.

Van Ark, E.M., Detrick, R.S., Canales, J.P., Carbotte, S.M., Harding, A.J., Kent, G.M., Nedimovic, M.R., Wilcock, W.S.D., Diebold, J.B., and Babcock, J.M., 2007, Seismic structure of the Endeavour Segment, Juan de Fuca Ridge: Correlations with seismicity and hydrothermal activity: Journal of Geophysical Research-Solid Earth, v. 112, B02401.

Von Damm, K.L., Oosting, S.E., Kozlowski, R., Buttermore, L.G., Colodner, D.C., Edmonds, H.N., Edmond, J.M., and Grebmeier, J.M., 1995, Evolution of East Pacific Rise hydrothermal vent fluids following a volcanic eruption: Nature, v. 375, p. 47-50.

Von Damm, K.L., Buttermore, L.G., Oosting, S.E., Bray, A.M., Fornari, D.J., Lilley, M.D., and Shanks, W.C., 1997, Direct observation of the evolution of a seafloor 'black smoker' from vapor to brine: Earth and Planetary Science Letters, v. 149, p. 101-111.

Von Damm, K.L., Bray, A.M., Buttermore, L.G., and Oosting, S.E., 1998, The geochemical controls on vent fluids from the Lucky Strike vent field, Mid-Atlantic Ridge: Earth and Planetary Science Letters, v. 160, p. 521-536.

Von Damm, K.L., Lilley, M.D., Shanks, W.C., Brockington, M., Bray, A.M., O'Grady, K.M., Olson, E., Graham, A., Proskurowski, G., and Sou, E.P.R.S.P., 2003, Extraordinary phase separation and segregation in vent fluids from the southern East Pacific Rise: Earth and Planetary Science Letters, v. 206, p. 365-378.

Von Quadt, A., Erni, M., Martinek, K., Moll, M., Peytcheva, I., and Heinrich, C.A., 2011, Zircon crystallization and the lifetimes of ore-forming magmatic-hydrothermal systems: Geology, v. 39, p. 731-734.

Weis, P., and Driesner, T., 2013, The interplay of non-static permeability and fluid flow as a possible pre-requisite for supercritical geothermal resources: Energy Procedia, v. 40, p. 102 - 106.

Weis, P., Driesner, T., Heinrich, C.A., Coumou, D., and Geiger, S., 2010, Flow of brine and vapour in subaerial and submarine magmatic hydrothermal systems: Smart Science for Exploration and Mining, Proceedings of the 10th Biennial SGA Meeting, v. 1., p. 873-875.

Weis, P., Driesner, T., and Heinrich, C.A., 2012, Porphyry-copper ore shells form at stable pressure-temperature fronts within dynamic fluid plumes: Science, v. 338, p. 1613-1616.

Weis, P., Driesner, T., and Heinrich, C.A., 2013, Temporal and spatial relationships between porphyry and epithermal systems: A hydrological perspective: Mineral Deposit research for a high-Tech World, Proceedings of the 12th Biennial SGA Meeting, p. 903-905.

Weis, P., Driesner, T., Coumou, D., and Geiger, S., 2014, Hydrothermal, multiphase convection of H_20-NaCl dluids from ambient to magmatic temperatures: A new numerical scheme and benchmarks for code comparison: Geofluids, doi: 10.1111/gfl.12080.

Wilkinson, J.J., 2013, Triggers for the formation of porphyry ore deposits in magmatic arcs: Nature Geoscience, v. 6, p. 917-925.

Williams-Jones, A.E., and Heinrich, C.A., 2005, 100th Anniversary special paper: Vapor transport of metals and the formation of magmatic-hydrothermal ore deposits: Economic Geology, v. 100, p. 1287-1312.

Yardley, B.W.D., 2005, 100th Anniversary Special Paper: Metal concentrations in crustal fluids and their relationship to ore formation: Economic Geology, v. 100, p. 613-632.

Zoback, M.D., Townend, J., and Grollimund, B., 2002, Steady-state failure equilibrium and deformation of intraplate lithosphere: International Geology Review, v. 44, p. 383-401.